Author Manuscript

Author Manuscript

Author Manuscript

Author Manuscript

HHS Public Access

Author manuscript

Biochemistry. Author manuscript; available in PMC 2023 March 29.

Published in final edited form as:

Biochemistry. 2023 March 21; 62(6): 1124–1137. doi:10.1021/acs.biochem.2c00685.

Biochemical Studies of Systemic Lupus Erythematosus-Associated Mutations in Nonreceptor Tyrosine Kinases Ack1 and Brk

Yagmur Kan[#],
Department of Physiology and Biophysics, School of Medicine, Stony Brook University, Stony Brook, New York 11794-8661, United States

YiTing Paung[#],
Department of Pharmacology, School of Medicine, Stony Brook University, Stony Brook, New York 11794-8661, United States

Yunyoung Kim,
Department of Physiology and Biophysics, School of Medicine, Stony Brook University, Stony Brook, New York 11794-8661, United States

Markus A. Seeliger,
Department of Pharmacology, School of Medicine, Stony Brook University, Stony Brook, New York 11794-8661, United States

W. Todd Miller
Department of Physiology and Biophysics, School of Medicine, Stony Brook University, Stony Brook, New York 11794-8661, United States; Department of Veterans Affairs Medical Center, Northport, New York 11768, United States

Abstract

Tyrosine kinases (TKs) play essential roles in signaling processes that regulate cell survival, migration, and proliferation. Dysregulation of tyrosine kinases underlies many disorders, including

Corresponding Authors: **Markus A. Seeliger** – *Department of Pharmacology, School of Medicine, Stony Brook University, Stony Brook, New York 11794-8661, United States;* markus.seeliger@stonybrook.edu; **W. Todd Miller** – *Department of Physiology and Biophysics, School of Medicine, Stony Brook University, Stony Brook, New York 11794-8661, United States; Department of Veterans Affairs Medical Center, Northport, New York 11768, United States;* todd.miller@stonybrook.edu.

[#]Author Contributions

Y.K. and Y.P. contributed equally to this work. The manuscript was written through the contributions of all authors. All authors have given their approval for the final version of the manuscript.

Supporting Information

The Supporting Information is available free of charge at https://pubs.acs.org/doi/10.1021/acs.biochem.2c00685.

Thermal shift assays, in vitro kinase inhibition assays, measurements of steady-state kinetic parameters, in silico predictions of the effects of the mutations, the activity of purified Ack1 K161Q toward various peptide substrates, distance difference matrix for Ack1 K161Q vs WT, multiple sequence alignment of TKs with homologous residues for Ack1 mutants, DynaMut model of Ack1 R247H (PDF)

Accession Codes

The X-ray coordinates and structure factors have been deposited in the Protein Data Bank as entry 8FE9. Ack1: Q07912. Brk: Q13882.

Complete contact information is available at: https://pubs.acs.org/10.1021/acs.biochem.2c00685

The authors declare no competing financial interest.

Author Manuscript Author Manuscript Author Manuscript Author Manuscript

cancer, cardiovascular and developmental diseases, as well as pathologies of the immune system. Ack1 and Brk are nonreceptor tyrosine kinases (NRTKs) best known for their roles in cancer. Here, we have biochemically characterized novel Ack1 and Brk mutations identified in patients with systemic lupus erythematosus (SLE). These mutations are the first SLE-linked polymorphisms found among NRTKs. We show that two of the mutants are catalytically inactive, while the other three have reduced activity. To understand the structural changes associated with the loss-of-function phenotype, we solved the crystal structure of one of the Ack1 kinase mutants, K161Q. Furthermore, two of the mutated residues (Ack1 A156 and K161) critical for catalytic activity are highly conserved among other TKs, and their substitution in other members of the kinase family could have implications in cancer. In contrast to canonical gain-of-function mutations in TKs observed in many cancers, we report loss-of-function mutations in Ack1 and Brk, highlighting the complexity of TK involvement in human diseases.

Graphical Abstract

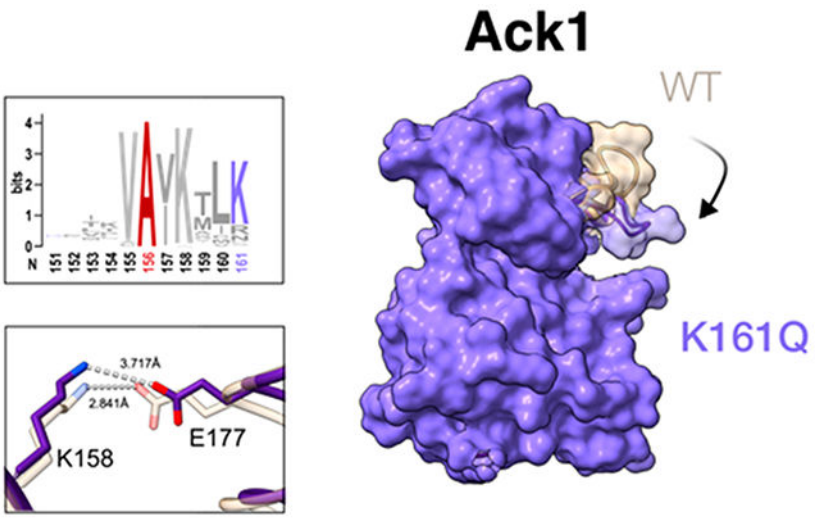

Tyrosine kinases (TKs) are ubiquitous enzymes that mediate crucial biological functions and regulate cell survival, activation, and differentiation pathways. Dysregulation of signaling cascades involving TKs often results in human diseases. Indeed, many proto-oncogenes are kinases that become inappropriately activated through gain-of-function mutations. For example, in Philadelphia chromosome-positive chronic myeloid leukemia, hyperactivating mutations in Abl kinase are linked to poor prognosis in response to imatinib therapy.[1–5] Mutations in some TKs are especially valuable diagnostic and prognostic markers for leukemias and lymphomas, given the involvement of JAKs, TYK, ITK, BTK, and SYK tyrosine kinases in critical signaling pathways downstream of immune receptors.[6,7] Approximately 30% of patients with acute myeloid leukemia carry mutations in FLT3 tyrosine kinase, a negative prognostic marker associated with a higher risk of relapse.[8,9] Src family kinases are known to play a role in autoimmunity: Lyn-deficient mice develop systemic lupus erythematosus (SLE).[10] Hyperactivation of tyrosine kinases has been reported in T cells, B cells, and other cells of the innate and adaptive immune systems in SLE patients and animal models.[11]

Author Manuscript Author Manuscript Author Manuscript Author Manuscript

In a recent study, Geissmann and colleagues performed whole exome sequencing of a group of SLE patients and their healthy relatives. They identified autosomal recessive loss-of-function mutations in Ack1 (A156T and K161Q) and Brk kinases (G257A and G321R) in patients from two families with SLE.[12] Sequencing of another group of pediatric lupus patients led to the identification of an additional loss-of-function Ack1 mutant (R247H). These findings suggested that these two kinases play a role in normal immune cell function. The novel mutations identified in this genetic survey of patients have not been documented in other databases, such as the Catalogue of Somatic Mutations in Cancer (COSMIC) and Online Mendelian Inheritance in Man (OMIM), or databases of genomic variations, such as the Single Nucleotide Polymorphism Database (dbSNP), the Genome Aggregation Database (gnomAD), and the Human Gene Mutation Database (HGMD).

SLE is a polygenic autoimmune disease in which hyperactivation of B cells and overexpression of Toll-like receptors (TLR) lead to autoantibody production.[13] These autoantibodies target nuclear components (antihistone and antidouble-stranded DNA) that become accessible after their release into the extracellular space upon apoptosis. The presence of autoantibodies causes the immune system to attack healthy tissues, leading to inflammation and tissue damage in affected areas.[14] Furthermore, abnormal T cell activation and cytokine production are also hallmarks of SLE and may be critical for initiating and maintaining autoimmune reaction.[13] The symptoms in individuals range from mild to life-threatening.[15] Although the causes of SLE remain unknown, some studies have linked SLE to hormonal changes,[16] environmental factors,[17–23] and genetic factors.[24–26]

Activated Cdc42-associated tyrosine kinase Ack1 is a nonreceptor tyrosine kinase (NRTK) consisting of a kinase domain (KD) fused to a C-terminal SH3 domain. The SH3 is followed by a Cdc42 and Rac1 binding (CRIB) motif that selectively binds Cdc42 (Figure 1A, top). Ack1 is the only protein to share a stretch of ~200 residues homologous to the epidermal growth factor receptor family inhibitor Mig6. This portion of Ack1 is designated the Mig6 homology region (MHR). Following the MHR, a ubiquitin-associated (UBA) domain makes up the C-terminal regions of the Ack1 kinase, making it the only tyrosine kinase with a UBA. This arrangement of domains is unusual for an NRTK. Together with the C-terminal MHR and UBA domains of Ack1, the SH3 domain is proposed to have a regulatory role through autoinhibition of the kinase domain.[27,28]

Ack1 is involved in a wide range of signaling cascades.[30] Regulators of actin dynamics such as Cdc42, WASP, cortactin;[31] AKT,[32] histone demethylase KDM3,[33] and tumor suppressor Wwox are among the substrates of Ack1. Signal transducers STAT1, STAT3, and STAT5 are also targets for Ack1[34] and modulate transcription in stem cells, especially hematopoietic stem cells. In addition, Ack1 plays a role in the Toll-like receptor (TLR) pathways and mediates the inflammatory response by regulating the MAPK and NF-κB pathways.[45] Experimental data suggest that Ack1 overexpression significantly activates the TLR4, TLR7, and TLR9 pathways, whereas the depletion of Ack1 has the opposite effect.

Brk is a member of the Frk family of NRTKs (consisting of Brk, Srms, Frk, and Src42A), which is considered to be a subfamily of the Src family. Brk is distantly related to c-Src, with 46% amino acid identity.[35,36] Brk comprises an auto-inhibitory SH3 domain, an

Author Manuscript Author Manuscript Author Manuscript Author Manuscript

SH2 domain, and a catalytic domain[36] (Figure 1A, bottom). Brk is highly expressed in breast carcinomas compared to its low expression levels in healthy breast tissues.[37] In addition to contributing to breast cancer growth, migration, and invasion, Brk is involved in several other cellular processes, such as regulating EGFR turnover, tumor metastasis, and epithelial-mesenchymal transition. The functions of Brk are specific to the cell type in which it is expressed.[38] In healthy tissues, Brk promotes cellular differentiation and apoptosis and mediates migration. However, in cancerous tissues, Brk sensitizes cells to mitogenic signals and enhances proliferation and anchorage-independent survival. Brk is constitutively activated in transformed T and B cells, despite not being expressed in normal, unstimulated lymphocytes.[39] In colorectal cancer cells, Brk phosphorylates JAK2 to activate JAK2/STAT3 signaling, contributes to cell stemness, and confers resistance to chemotherapy.[40] Similar to Ack1, Brk activates STAT3 and STAT5 through phosphorylation, thereby enhancing the transcriptional activity of STATs.[44] However, the current knowledge of the roles of both Ack1 and Brk in immune cells is limited.

NRTKs such as Brk and Ack1 share a highly conserved catalytic KD, which has a bilobal architecture with an amino-terminal N-lobe and a carboxy-terminal C-lobe. The small N-lobe contains six (Ack1) or five (Brk) β-strands and a single α-helix called the αC helix, analogous to the PKA naming convention (Figure 1B,C).[41,42] The larger C-lobe is predominantly composed of helices. Between the two lobes lie the substrate peptide binding site and the ATP-binding site. Inside the ATP binding site, a gatekeeper threonine (T205 in Ack1, T264 in Brk) contributes to the selectivity for nucleotides and small-molecule inhibitors.[43] The highly conserved phosphate binding P-loop (Figure 1) contains a glycine-rich motif (GxGxG) and shields one side of the ATP-binding pocket from the solvent.[44] The substrate-binding site is adjacent to the αC helix, allowing the substrate peptide to come in contact with the γ-phosphate of ATP. The activation loop (20–30 residues) near the substrate-binding site contains a conserved Asp-Phe-Gly (DFG) motif (Figure 1), which contributes to ATP binding and controls whether the activation loop is in a conformation that is compatible with substrate peptide-binding.

There are two hallmarks of kinase activation: the repositioning of (1) the αC helix (Figure 1D) and (2) the DFG motif. In the active conformation, the Asp residue of the DFG motif points toward the ATP-binding pocket, where it binds Mg^{2+}/ATP. Additionally, the αC helix faces toward the active site, and a glutamate in the αC helix forms a salt bridge with catalytic lysine. Disruption of either of these structural hallmarks inactivates the kinases.

Here, we studied SLE-associated loss-of-function mutations in Ack1 (A156T, K161Q, and R247H) and Brk (G257A and G321R). These mutations have been identified in pediatric SLE patients with severe forms of the disease. The functional effects of the mutations Ack1 A156T, K161Q; Brk G257A and G321R have been previously studied using an induced pluripotent stem cell-derived in vitro model.[12] In the present study, we examined the biochemical properties and catalytic activity of these mutants and analyzed the structural changes associated with the mutations. We solved the crystal structure of the Ack1 KD K161Q mutant at a resolution of 3.2 Å. These studies explain the disruption of TK activity observed in loss-of-function mutations.

Author Manuscript Author Manuscript Author Manuscript Author Manuscript

MATERIALS AND METHODS

Reagents.

Bovine serum albumin, leupeptin (10 μ/mL), aprotinin (10 μ/mL), phenylmethylsulfonyl fluoride (200 μM), sodium orthovanadate (0.2 mM), dithiothreitol, pyruvate kinase/lactate dehydrogenase enzymes, and SYPRO Orange were obtained from Sigma. The P81 phosphocellulose paper was from Whatman, and [^{32}P] ATP was purchased from PerkinElmer. The peptides were purchased from Genemed Synthesis Inc. and purified by semipreparative HPLC on a Vydac C18 column, lyophilized, and resuspended in Tris-HCl buffer (pH 8.0), as previously.[45]

cDNAs and Site-Directed Mutagenesis.

Recombinant baculovirus constructs encoding full-length Brk and the His-tagged kinase domain of Ack1 were used for insect cell expression, according to our previous methods.[35,36,45,46] Mutations were introduced by site-directed mutagenesis using the QuikChange II kit (Agilent) and verified by DNA sequencing.

Protein Purification.

The Ack1 kinase domain (UniprotKB, Q07912) and full-length Brk (SH3-SH2-kinase) (UniprotKB, Q13882) were purified from *Spodoptera frugiperda* Sf9 cells by chromatography on Ni-NTA columns (Qiagen), as previously described.[35,46] For crystallization, the protein was further purified by size exclusion chromatography on a Superdex 200 (16/60) column, with a buffer consisting of 25 mM Hepes (pH 7.7), 300 mM NaCl, 0.5 mM TCEP, 20 mM $MgCl_2$, and 10% Glycerol.

Kinase Activity Assays.

Steady-state kinetic measurements of purified Ack1 and Brk kinase activity were performed using a continuous spectrophotometric ATP regeneration assay. The reactions were carried out at 30 °C in a final volume of 75 μL with 0.5 μM enzyme. The synthetic peptide substrate for Ack1 was derived from Wiskott-Aldrich syndrome protein (WASP) (KVIYDFIEKKKG),[46] and a Src-specific peptide (AEEEEIYGEFEAKKKKG) was used as a substrate for Brk. The reactions contained 100 mM Tris (pH 7.4), 10 mM $MgCl_2$, 1 mM phosphoenolpyruvate (PEP), 90 units/mL pyruvate kinase, 109 units/mL lactate dehydrogenase, 1.2 mg/ mL NADH, and varying amounts of ATP. The reduction in NADH absorbance was measured at 340 nm using a VersaMax plate reader. Initial rates were measured in triplicate, and kinetic parameters were determined by fitting the data to the Michaelis–Menten equation using nonlinear regression analysis (GraphPad Prism).

Phosphocellulose Paper Binding Assay.

Kinase activity was measured using phosphocellulose paper binding assays with purified proteins and [γ^{32}P]ATP. The reactions contained 20 mM Tris-HCl (pH 7.4), 10 mM $MgCl_2$, 0.25 mM ATP and 20–50 cpm/pmol of [γ^{32}P]ATP. The peptides used in this assay are Wiskott-Aldrich syndrome protein (WASP) (KVIYDFIEKKKG)[46] peptide for Ack1 and a Src-specific peptide (AEEEEIYGEFEAKKKKG) for Brk at a concentration of 1 mM.

Author Manuscript Author Manuscript Author Manuscript Author Manuscript

Reactions were carried out at 30 °C for 15 min with 1 μM Ack KD or Brk FL (SH3-SH2-KD). Kinase inhibition assays were performed using 500 nM enzyme (Ack KD or Brk FL), 200 μM ATP, 10 μM (R)-9b or dasatinib, and 1 mM peptide (WASP for Ack1, Src-specific peptide for Brk). Reactions were carried out for 10 min at 30 °C.

Crystallization.

The crystallization conditions were screened by the hanging drop method using a 3-drop 96-well Intelli-Plate prepared using the NT8 Drop Setter (Formulatrix Inc.) at 4 °C. Buffer screens were based on previously established conditions for wild-type Ack1 complexes with (R)-9b, and were performed using a nanoliter volume liquid handling platform (Formulatrix Inc.). Ack1 (3 mg/mL) was incubated with the ATP-competitive inhibitor (R)-9b at a 1:2 protein-drug ratio for 1 h before mixing with the reservoir liquid. The total volume of each drop was 400 nL, made up of Ack1 protein and reservoir liquid in a 1:1 ratio, and a transparent tape was used to seal the wells. All the plates in the crystallography imager (Formulatrix Inc.) were stored at room temperature.

For the K161Q mutant, promising crystals from the plate (0.05 M Bis-Tris pH 6.0–6.2, 19–24% PEG3350, 0.2–0.3 M $MgCl_2$, 2.5% glycerol) were crushed using the crystal-crushing tool and diluted to 50 μL with the reservoir solution of the crushed crystal. The diluted crushed crystals were vortexed for 3 min and used as the original seed stock. The original seed stock was serially diluted to 1:10, 1:100, and 1:1000, which served as the crystal seed when preparing the crystallization screen in a Falcon 24-well plate. The crystallization hanging drop was prepared on an 18 mm siliconized glass circle cover slide (Hampton Research), with each drop containing 1 μL of 3 mg/mL Ack1 protein, 0.66 μL of reservoir liquid from the well, and 0.34 μL of seed stock. All crystal plates were stored at room temperature and monitored daily using confocal microscopy. The best crystal from this step was used as the seed stock for the next crystallization plate. The second seeding cycle yielded large needles for K161Q, which were used for crystal shooting. The best crystal was obtained in a buffer composed of 0.05 M Bis-Tris (pH 5.8), 19% PEG3350, 0.3 M $MgCl_2$, and 2.5% glycerol.

X-ray Diffraction.

The X-ray diffraction data were collected at the National Synchrotron Light Source II (NSLS-II). The K161Q crystal diffraction pattern was obtained at 100 K and a wavelength of 0.98 Å with the following parameters: oscillation width, 0.2; exposure time, 0.02; transmission, 0.3; oscillation range, 0–360°; detector distance, 270 mm; and protocol, vector.

Structural Determination and Refinement.

The K161Q diffraction pattern was processed using XDS[47–55] and solved by molecular replacement[56] using the structure of wild-type Ack1 (Protein Data Bank, PDB: 4EWH) as a search model. The Ack1 K161Q model was built and refined using Coot[57] and PHENIX,[58] respectively. The diffraction data collection and refinement statistics are summarized in Table 1. The UCSF Chimera tool RRDistMaps[59] was used to generate the distance-difference matrix shown in Figure S5.

Author Manuscript Author Manuscript Author Manuscript Author Manuscript

Thermal Shift Assays.

The thermal melting temperatures of Ack1 and Brk proteins were measured by fluorescence using SYPRO Orange (Sigma) at a 5× concentration. The quantum yield of the dye increases when it binds to the exposed hydrophobic surfaces of denatured proteins. The proteins were heat-denatured from 5 to 95 °C, and fluorescence emission spectra (excitation/emission 470 nm/570 nm) were recorded at 2 °C intervals in a StepOne Real-Time PCR System (Applied Biosystems).

Multiple Sequence Alignment.

SLE-associated residues of interest were isolated from the structurally guided kinase family sequence alignment by Modi and Dunbrack.[29] Each member of the alignment with a homologous residue (94 tyrosine kinases) was searched for in the COSMIC database to generate Table 2. Alignments were depicted using JalView software.[60] The ClustalX coloring scheme was used to represent the chemical characteristics of amino acids, where hydrophobic residues (Ala, Cys, Phe, Ile, His, Leu, Met, Val, Trp, and Tyr) with >60% conservancy are represented in blue; negatively charged residues (Asp and Glu) with >50% conservancy are colored magenta; positively charged Arg and Lys with >60% conservancy are highlighted in red. Polar residues (Ser, Thr, Gln, and Asn) with at least 50% conservancy are colored green, and cysteine and glycine residues with at least 85% conservancy are colored pink and orange, respectively. The aromatic residues (Phe, Tyr, Trp) are cyan.

DynaMut Simulation and *in Silico* Analysis of Mutations.

We performed a DynaMut[61] simulation to predict the effect of a point mutation on the flexibility of the WT protein. DynaMut is a web server-based software that implements Normal Mode Analysis (NMA), which predicts the dynamics of a system around a conformation through harmonic motion. The structural model used in the analysis was downloaded from the PDB (ID: 4EWH). Before analysis, water, inhibitors, and cofactors were removed from the reference PDB models. The point mutation was defined using the built-in function of the software.

In silico analysis was performed to identify the effects of the mutations on the function, stability, and structure of the enzymes (Figure 3). Sorting Intolerant from Tolerant “SIFT” (https://sift.bii.a-star.edu.sg/)[62] was used to predict the functional effect of mutations. FoldX,[63] Impact of Non-synonymous mutations on Protein Stability “INPS-3D” (https://inpsmd.biocomp.unibo.it/inpsSuite/default/index3D),[64] Single Amino Acid Folding free Energy Changes “SAAFEC-SEQ” (http://compbio.clemson.edu/SAAFEC-SEQ/),[65,66] PoPMuSiC (https://soft.dezyme.com/query/create/pop),[67] the recently developed protein stability predictor “PROST” (https://github.com/ShahidIqb/PROST) were utilized to check the thermodynamic stability of the proteins upon mutation.

RESULTS

Systemic Lupus Erythematosus-Associated Mutations Impact Kinase Activity.

Loss-of-function mutations in the nonreceptor tyrosine kinases Ack1/TNK2 (A156T, K161Q, R247H) and Brk/PTK6 (G257A, G321R) have been identified in patients with

Author Manuscript Author Manuscript Author Manuscript Author Manuscript

systemic lupus erythematosus.[12] While the Ack1 A156T and K161Q mutations are in the N-lobe of the kinase, the R247H mutation is in the C-lobe. Both A156 and K161 are located within the β4-sheet of the N-lobe and are highly conserved among NRTKs (Figure 1E). The Brk G257A (dark blue) and G321R (purple) mutations fall in the kinase N-lobe (Figure 1C).

To examine the effects of the mutations, we expressed the corresponding mutant proteins in Sf9 insect cells. For Ack1 (wild-type and mutants), we expressed and purified the kinase catalytic domain. For Brk, we expressed and purified the full-length wild-type (WT) and mutant kinases. We previously showed that these proteins are predominantly in their unphosphorylated state following purification from Sf9 cells.[36,68] Our initial screening for catalytic activity showed that Ack1 A156T and Brk G321R were kinase-dead mutants, while Ack1 K161Q and Brk G257A were severe loss-of-function mutants with a small amount of residual activity (Figure 2A,B).

Mutant Proteins Have Altered Stability but Still Bind to Inhibitors.

We utilized several bioinformatic tools to predict changes in thermodynamic stability ($\Delta\Delta G$) upon mutation. FoldX, DeepDDG, and other stability predictors show similar trends regarding expected changes in $\Delta\Delta G$ (Figure 3).

Substitution mutations often reduce the stability of the protein structure by reducing or overpacking the hydrophobic core with larger side chains, introducing strain, or loss of electrostatic interactions in monogenic diseases.[70] We compared the melting temperatures of purified Ack1 KD and full-length Brk proteins using thermal shift assays to determine the effects of mutations on the thermodynamic stability of the proteins (Figures 4 and S1). The A156T and R247H mutations in Ack1 decreased the melting temperature (Figures 4A and S1A), suggesting that these mutants destabilize the kinase. In contrast, the K161Q mutation in Ack1 increases the melting temperature. The $\Delta\Delta G$ predictions obtained from the computational tools (Figure 3) for the effects of mutations on protein stability agree with these results such that increasing T_m (higher stability) is positively correlated with smaller $\Delta\Delta G$.

Most ligands and inhibitors stabilize proteins when bound to a folded protein, leading to an increase in unfolding temperature. The melting temperatures of all mutants, including Ack1 K161Q, increased with the ATP-competitive inhibitor (R)-9b, suggesting that the mutants could bind to (R)-9b, as evidenced by their stabilization by the inhibitor (Figures 4B and S1B). We confirmed the abilities of the Ack1 K161Q and R247H mutants to bind (R)-9b by an in vitro kinase inhibition assay (Figure S2).

The lupus-associated Brk mutants G257A and G321R had a significantly lower T_m than WT, while G321R exhibited a more drastic decrease in T_m (Figures 4C and S1C). The melting temperature of G257A increased in the presence of dasatinib, indicating its binding (Figures 4D and S1D). An in vitro kinase inhibition assay verified the ability of the G257A mutant to bind dasatinib (Figure S2). The decrease in T_m was in agreement with the expected destabilization assessed by DeepDDG and SAAFEC-SEQ.

Author Manuscript Author Manuscript Author Manuscript Author Manuscript

Mutations Reduce Kinase Activity and Affect Substrate Saturability.

To measure Ack1 kinase activity, we used a continuous spectrophotometric assay. The assay showed an expected linear relationship between enzyme concentration and activity on enzyme progress curves (Figure S3A). We used this assay to measure steady-state kinetic values for the wild-type, K161Q, and R247H forms of Ack1 (Figure S3, panels B–D), wild-type and G257A forms of Brk (Figure S3, panels E–F). The A156T and G321R mutants did not show detectable activity in this assay, consistent with the results of the phosphocellulose binding assay with [γ^{32}P] (Figure 2).

As shown in Figure 5A, the V_{max} values for mutants K161Q and R247H were 19.6 and 13.9 mOD/min, respectively, compared to 45.5 mOD/min for wild-type Ack1. The mutants showed differential effects on K_m (ATP); the K161Q mutant had 1.7 times higher K_m (ATP) than wild-type Ack1, while the R247H mutant had a 33% reduction in K_m (ATP) (Figure 5B). We used the continuous assay to measure apparent K_m (peptide) values for wild-type Ack1 and the mutants (Figure S4). The K_m for the WASP peptide was in the millimolar range for these Ack1 constructs, and we were not able to achieve saturation because of solubility constraints. The value for K_m (peptide) was somewhat higher for K161Q (2.96 mM) than for WT (2.21 mM) (Figure S4A vs S4B), while the estimated K_m (peptide) for R247H was much higher (~7 mM) (Figure S4C).

The Brk mutant G257A exhibited a V_{max} value close to that of WT (Figure 5C). Differences in kinetic parameters between this mutant and WT were not statistically significant, suggesting additional mechanisms for the loss-of-activity phenotype.

Crystallographic Analysis of the SLE-Associated Mutant Ack K161Q Provided Insights into Its Impaired Catalytic Activity.

We solved the X-ray crystal structure of Ack1 kinase domain harboring the K161Q mutation (Table 1). Several structural differences were evident between WT and K161Q Ack1. We observed the repositioning of the αC-ß4 Loop in K161Q with respect to that of the WT (Figures 6A and S5). This loop is highly conserved among eukaryotic protein kinases,[71] such that changes in the αC-ß4 loop position might contribute to the decrease in activity (Figures 2 and 4) through the steric hindrance of the substrate-binding site. In the active WT KD, this loop points toward the solvent away from the active site (Figures 1D and 6B, beige), while it expands to accommodate the shift in the αC-helix in the inactive conformation (Figures 1D and 6B, gray). Similar to the position of the αC-helix in the inactive kinase structure, the αC-helix of K161Q is also shifted outward (Figure 6B,C). The position of the αC-helix impacts the activity of TKs by enabling or disabling a highly conserved salt bridge between the catalytic lysine (K158 of Ack1) and conserved glutamate (E177 of Ack1) of the αC-helix. In active WT KD, the αC-helix is pointed inward, closer to the substrate-binding cleft (Figures 1D and 6B, beige), while it rotates outward in the inactive conformation (Figures 1D and 6B, gray). Therefore, we compared the αC-helix position of Ack1 K161Q to that of active and inactive Ack1. Our structure revealed a slight shift in the αC-helix away from the kinase core, similar to that of the inactive WT (Figures 6B and 1D, purple vs gray). This shift may be caused by αC-ß4 loop relocation, also disturbing the K158-E177 salt bridge (Figure 6C, inset). The interaction is weaker in K161Q

Author Manuscript Author Manuscript Author Manuscript Author Manuscript

(3.7 Å) than in WT Ack1 (2.8 Å). The shift in the αC helix also introduces new H bonds between the backbone nitrogen of G167 (of αC helix) and its backbone carbonyl oxygen (Figure 6D).

In the mutant structure, repositioning of the αC-ß4 loop favors novel interactions absent in the WT; the carbonyl group of the Q161 side chain forms an H-bond with the V139 amide proton of the backbone (Figure 6E, 3.5 Å). Furthermore, this interaction between Q161-V139 pushes the αC-β4 loop toward the C-lobe, resulting in partial occupation of the substrate-binding site (Figure 6A). The Ack1 WT structure lacks this interaction, as the K161 side chain is more flexible and points away from V139.

In addition to the αC-ß4 loop repositioning, the K161Q mutant favors a salt bridge between E169 and R176 (Figure 6F). E169 of the mutant points toward the substrate-binding site, which sterically hinders part of the substrate-binding site. In the active form of WT Ack1, E169 faces away from the substrate-binding site, making this salt bridge unfavorable. Interestingly, this interaction is present in the inactive conformation, which supports our experimental data showing a loss of kinase activity. Movement of the N-terminus of the αC-helix is a crucial step for catalysis, such that the position of the N-terminus of the αC-helix relative to the activation loop determines whether an open conformation is achieved for substrate binding.[72,73] Because we observed a shift in the position of the αC-helix (Figure 6B) concomitant with loss of activity, we considered a possible change in substrate specificity. We tested the catalytic activity of Ack1 K161Q toward other peptide substrates (Figure S6). The Abl peptide is known to be a suboptimal substrate for WT Ack1, the second-best peptide substrate (after WASP),[45] while other peptides included in the study are ideal substrates for other tyrosine kinases, as indicated. Ack1 K161Q did not exhibit any substrate preference different from WT, and the WASP peptide remained the best substrate tested (Figure S6). The A-loop and DFG motif conformations of the K161Q mutant remained the same as those of the active WT protein (Figure 6C). This observation is not surprising, as Ack1 K161Q retains residual activity in our assays.

The N-lobe has been suggested to symmetrically dimerize, and the N-terminal SAM domains cooperatively facilitate dimerization.[28] N-terminal truncations in Ack1 significantly alter its catalytic activity.[68] As the K161Q mutation alters the N-lobe conformation, it could also potentially affect the dimerization and kinase activity of the full-length protein.

Overall, the K161Q mutant adopts structural characteristics that are intermediate between those of the active and inactive conformations. Compared to the autoinhibited inactive structure of c-Src (PDB: 2SRC) and the active structure of Ack1 (PDB: 4EWH), the αC-ß4 Loop of K161Q is positioned between that of inactive c-Src and active Ack1. F271 of the DFG motif and A-loop of the kinase take up the active conformation. The loss of the conserved salt bridge between αC Glu (E177) and ß4 Lys (K158) (Figure 6C), partial occlusion of the substrate-binding site, the formation of new hydrogen bonds, and salt bridges (Figure 6E,F) further stabilize the inactive-like characteristics.

Author Manuscript Author Manuscript Author Manuscript Author Manuscript

Mutated Residues Are Conserved among Tyrosine Kinases.

We analyzed the sequence conservation of these mutated residues among other tyrosine kinases. We found that K161 of Ack1 was conserved in 67% of the 94 tyrosine kinases analyzed. Although this lysine is not conserved in the Ack family kinase Tnk1, its basic nature is maintained with arginine. Other tyrosine kinases that possess arginine at the equivalent position are NRTKs, FES, ITK, and TEC (Figure S7A), and RTKs DDR1, DDR2, EGFR, ERBB2, Eph receptors A10 and B2 (Figure S7B). Interestingly, the insulin receptor family has asparagine at this position, together with the Met and TXK receptor tyrosine kinases.

A156T is located within the ATP-binding site and is the alanine residue of the conserved AXK motif in the β4 strand of Ack1 (Figure 1E), while it is in the β3 strand of most kinases. A156 is a part of the catalytic spine and contributes to the positioning of ATP. Together with V140 of β3 within the catalytic spine, Al56 is positioned directly onto the adenine ring of ATP. Therefore, it is highly conserved among the TKs (Figures 1E and S7A–B).

G257 of Brk is shared by the Src-like kinase Srms. This residue is more conserved in RTKs (Axl, EphA7, EphA8, EphA10; FGFR3, insulin family RTKs, MUSK, TRKA-C, TYK2, CSF1R, KIT, PDGFRB) than in NRTKs (JAK2 and JAK3) (Figure S8A). Brk G321 is present in closely related Src family kinases (Frk, Fyn, Fgr, Src, Yes1), the Abl family (Abl1, Abl2), ITK, RTK family DDR (DDR1, DDR2), FER, TRKA-C, TIE family (TEK, TIE1), MUSK, and ROR1 (Figure S8B).

Ack1 R247 is not conserved within NRTKs (Abl, Fyn, Lyn, Hck, and Src) but is conserved in EGFR (Figure S7C). Although Arg is not necessarily conserved, the interaction between the A loop and the equivalent residue is observed in these kinases. For example, in active Abl, the side chain of the equivalent residue (N358) interacts with the carbonyl group of G390. In active EGFR, the R832 side chain interacts with the backbone carbonyl groups of G863, A864, and E866; the backbone carbonyl group of R832 interacts with the backbone amine of L862. Therefore, mutating R247 to His could potentially abolish these interactions and have a destabilizing effect. To test this hypothesis, we performed flexibility predictions using DynaMut. The predicted model for R247H reveals an increase in the flexibility of the A-loop compared to that of WT (Figure S9). The mutation of R247 to His is predicted to alter the flexibility of the protein structure. The simulation suggests a significant increase in flexibility on the A-loop of the R247H mutant. This observation could contribute to the loss of Ack1 activity observed under the conditions tested in this study and in patients with SLE.

The loss of activity might arise from the loss of interaction between R247 and A-loop residues. In the WT structure, R247 interacts with the backbone of the A loop residues D281, P278, and L277 (Figure S9). This interaction enables the A-loop to remain in the active conformation. However, the simulated model showed that mutation of R247 to His disabled these interactions (Figure S9). Without these interactions, the A-loop gains flexibility and flips between the active and inactive conformations, causing suppression in activity.

Author Manuscript Author Manuscript Author Manuscript Author Manuscript

DISCUSSION

In this study, we examined the biochemical characteristics of the SLE-associated mutations A156T, K161Q, and R247H in Ack1, and G257A and G321R in Brk. We solved the crystal structure of Ack1 K161Q, which revealed a conformation possessing the characteristics of both the active and inactive kinase structures. Because this mutant retains ~35% activity (Figure 2A), the crystal structure provides information on the partial loss of Ack1 activity (Figure 6). The distance between catalytic Lys and Glu in αC is 2.8 Å in the active structure (PDB: 4EWH) and 3.7 Å in K161Q (Figure 6C, inset). The largest difference is observed in the αC-ß4 loop. This loop changes from being solvent-facing in the WT structure to activation loop-facing in the mutant form, moving toward the C-lobe (Figure S5). This movement results in maximum displacements in the Cα of L165 by 11.7 Å (Figure S5).

We observed a significant decrease in the thermal stability of A156T compared to that of WT (Figure 4A), thus providing an explanation for the functional loss of the mutant. The DynaMut simulation for Ack1 R247H suggests a more flexible A-loop compared to the WT (Figure S9), suggesting the destabilization of the active conformation. Overall, these observations shed light on the complete or partial loss of activity in Ack1 observed among SLE patients harboring the mutations analyzed in this study.

The in silico thermostability calculations for Ack1 follow a consistent trend between each algorithm and agree with the experimental data. In contrast, the predictions of FoldX, INPS-3D, PoPMuSiC, and PROST for Brk do not match the experimental values, as the G321R is a more destabilizing mutation than G257A Some of these in silico tools use energy functions to compute the $\Delta\Delta G$ (e.g., FoldX), whereas others have machine-learning approaches and rely on data set training (e.g., DeepDDG and PoPMuSiC). DeepDDG was trained on more than 5700 experimental data points.[74] DeepDDG considers the solvent-accessible surface area of the mutated residue as the most important feature, which could explain why it accurately assessed G321R vs G257A. PoPMuSiC's algorithm similarly depends on solvent accessibility; the difference in performance vs DeepDDG could be due to the specific data sets used to train these programs.

The discrepancy between the experimental data and the bioinformatic predictions demonstrates that a single algorithm may not perform equally accurately even within the same subfamily of proteins (nonreceptor tyrosine kinases). Indeed, one study evaluating the performance of 11 different stability prediction tools used 1784 single mutations occurring in 80 proteins as input and showed that there was not a single mutation in which all of the programs correctly predicted the experimental result.[75] Our results with Brk similarly highlight the limitations of the stability predictors. In addition, while we assume that a loss-of-function mutation should be destabilizing, we note that there is evidence in the literature that some disease-associated mutations increase protein stability.[76]

Mutated residues identified in Ack1 and Brk are crucial for maintaining kinase activity. In Table 2, we summarize the analogous mutations identified in other kinases. EGFR R832H (equivalent to Ack1 R247H) has been identified in bone and kidney cancers.[77] EGFR A743T (analogous to Ack1 A156T) has been identified in lung and upper aerodigestive

Author Manuscript Author Manuscript Author Manuscript Author Manuscript

tract cancers.[87,98] Residues equivalent to Brk G321R (G372R in Abl 1a and G391R in Abl 1b) have been identified as imatinib-resistant mutants.[83,84] However, there is minimal information regarding these mutants, and further investigation is required to characterize the effects of these mutations.

Loss-of-function mutations in Ack1 can also impact TLR signaling cascades. These signaling pathways are known to participate in aberrant immune responses. In this regard, the role of Ack1 in TLR activation pathways and autoimmune diseases has recently been reported.[99] In mouse models of SLE, Ack1 inhibition was shown to alleviate lupus-like syndromes.[99] In contrast, the SLE-associated mutations studied here involve decreased Ack1 function, indicative of an alternative mechanism underlying the pathogenesis of this complex polygenic disease. The diversity of genetic backgrounds in SLE could affect the modus operandi for Ack1 (or Brk) in immune cells, suggesting that the nature of the involvement of tyrosine kinases is context-dependent. A similar discordance is observed in EGFR-dependent cancers, where downregulation of the Ack1 oncogene promotes drug resistance by increasing the half-life of EGFR.[100] Likewise, wild-type proteins could contribute to SLE pathology under susceptible conditions, while loss-of-function mutations could serve as compensatory surrogate pathways for disease progression depending on genetic predisposition.

Additional studies are needed to address the potential cellular mechanisms underlying the loss-of-function mutations in Ack1 and Brk. Because Ack1 is an activator of Akt and STAT, loss of Ack1 function could negatively impact these signaling pathways. The deactivation of Akt and STAT is associated with a loss of the anti-inflammatory response and a decrease in apoptotic cell uptake, which is phenotypic in patients with SLE. Brk phosphorylates and downregulates Dok1, a protein associated with autoimmune response. However, the mechanism by which Brk influences T cell regulation through Dok1 might involve other proteins.

Although the roles of Ack1 and Brk1 in autoimmunity remain unknown, our findings suggest that SLE-associated Ack1 mutations affect specific activities and destabilize the enzymes. Our study broadens our understanding of mutations in the NRTKs Ack1 and Brk, which tend to be characterized as gain-of-function mutations in disease contexts. We showed that the two residues (Ack1 A156 and K161) critical for catalytic activity are also highly conserved among other TKs (Figures 1E and S7A–B), providing further evidence that mutations in these residues might not be tolerated in the other members of the TK family.

Supplementary Material

Refer to Web version on PubMed Central for supplementary material.

ACKNOWLEDGMENTS

We thank Terrence Jiang for assistance with crystallography experiments. This research used resources of the National Synchrotron Light Source II, a U.S. Department of Energy (DOE) Office of Science User Facility operated for the DOE Office of Science by Brookhaven National Laboratory under Contract No. DE-SC0012704.

Author Manuscript Author Manuscript Author Manuscript Author Manuscript

Funding

This work was funded by the National Institute of General Medical Sciences of the National Institute of Health (NIH) under award number R35GM119437 to M.A.S., by the National Institute of Allergy and Infectious Diseases, NIH under award number R01AI164424 to W.T.M, and the VA Merit Award #BX002292 to W.T.M.

ABBREVIATIONS

TK	tyrosine kinase
NRTK	nonreceptor tyrosine kinase
RTK	receptor tyrosine kinase
SLE	systemic lupus erythematosus
COSMIC	Catalogue of Somatic Mutations in Cancer
OMIM	Online Mendelian Inheritance in Man
dbSNP	Single Nucleotide Polymorphism Database
gnomAD	The Genome Aggregation Database
HGMD	Human Gene Mutation Database
KD	kinase domain
CRIB	Cdc42, and Rac1 binding
SH3	Src homology 3
MHR	Mig6 homology region
UBA	ubiquitin-associated
TLR	Toll-like receptor
HEK	human embryonic kidney

REFERENCES

(1). Cross NC; White HE; Muller MC; Saglio G; Hochhaus A Standardized definitions of molecular response in chronic myeloid leukemia. Leukemia 2012, 26, 2172–2175. [PubMed: 22504141]

(2). Greuber EK; Smith-Pearson P; Wang J; Pendergast AM Role of abl family kinases in cancer: From leukaemia to solid tumours. Nat. Rev. Cancer 2013, 13, 559–571. [PubMed: 23842646]

(3). Kuntz EM; Baquero P; Michie AM; Dunn K; Tardito S; Holyoake TL; Helgason GV; Gottlieb E Targeting mitochondrial oxidative phosphorylation eradicates therapy-resistant chronic myeloid leukemia stem cells. Nat. Med 2017, 23, 1234–1240. [PubMed: 28920959]

(4). Marin D; Ibrahim AR; Lucas C; Gerrard G; Wang L; Szydlo RM; Clark RE; Apperley JF; Milojkovic D; Bua M; Pavlu J; Paliompeis C; Reid A; Rezvani K; Goldman JM; Foroni L Assessment of bcr-abl1 transcript levels at 3 months is the only requirement for predicting outcome for patients with chronic myeloid leukemia treated with tyrosine kinase inhibitors. J. Clin Oncol 2012, 30, 232–238. [PubMed: 22067393]

(5). Shanmuganathan N; Pagani IS; Ross DM; Park S; Yong ASM; Braley JA; Altamura HK; Hiwase DK; Yeung DT; Kim DW; Branford S; Hughes TP Early bcr-abl1 kinetics are predictive of

Author Manuscript Author Manuscript Author Manuscript Author Manuscript

subsequent achievement of treatment-free remission in chronic myeloid leukemia. Blood 2021, 137, 1196–1207. [PubMed: 32871588]

(6). Nag K; Chaudhary A Mediators of tyrosine phosphorylation in innate immunity: From host defense to inflammation onto oncogenesis. Curr. Signal Transduct Ther 2009, 4, 76–81. [PubMed: 21709741]

(7). Zarrin AA; Bao K; Lupardus P; Vucic D Kinase inhibition in autoimmunity and inflammation. Nat. Rev. Drug Discov 2021, 20, 39–63. [PubMed: 33077936]

(8). Döhner H; Weisdorf DJ; Bloomfield CD Acute myeloid leukemia. New England Journal of Medicine 2015, 373, 1136–1152. [PubMed: 26376137]

(9). Nagel G; Weber D; Fromm E; Erhardt S; Lubbert M; Fiedler W; Kindler T; Krauter J; Brossart P; Kundgen A; Salih HR; Westermann J; Wulf G; Hertenstein B; Wattad M; Gotze K; Kraemer D; Heinicke T; Girschikofsky M; Derigs HG; Horst HA; Rudolph C; Heuser M; Gohring G; Teleanu V; Bullinger L; Thol F; Gaidzik VI; Paschka P; Dohner K; Ganser A; Dohner H; Schlenk RF Epidemiological, genetic, and clinical characterization by age of newly diagnosed acute myeloid leukemia based on an academic population-based registry study (amlsg bio). Ann. Hematol 2017, 96, 1993–2003. [PubMed: 29090343]

(10). Hibbs ML; Tarlinton DM; Armes J; Grail D; Hodgson G; Maglitto R; Stacker SA; Dunn AR Multiple defects in the immune system of lyn-deficient mice, culminating in autoimmune disease. Cell 1995, 83, 301–311. [PubMed: 7585947]

(11). Shao WH; Cohen PL The role of tyrosine kinases in systemic lupus erythematosus and their potential as therapeutic targets. Expert Rev. Clin Immunol 2014, 10, 573–582. [PubMed: 24678775]

(12). Guillet S (2019) Monogenic Predisposition to Systemic Lupus Erythematosus and Efferocytosis; PhD Thesis, Université Sorbonne-Paris-Cité, Paris.

(13). Fillatreau S; Manfroi B; Dorner T Toll-like receptor signalling in b cells during systemic lupus erythematosus. Nat. Rev. Rheumatol 2021, 17, 98–108. [PubMed: 33339987]

(14). Love PE; Santoro SA Antiphospholipid antibodies: Anticardiolipin and the lupus anticoagulant in systemic lupus erythematosus (sle) and in non-sle disorders. Prevalence and clinical significance. Ann. Int. Med 1990, 112, 682–698. [PubMed: 2110431]

(15). Carter EE; Barr SG; Clarke AE The global burden of sle: Prevalence, health disparities and socioeconomic impact. Nat. Rev. Rheumatol 2016, 12, 605–620. [PubMed: 27558659]

(16). Ostensen M Sex hormones and pregnancy in rheumatoid arthritis and systemic lupus erythematosus. Ann. N.Y. Acad. Sci 1999, 876, 131–143. [PubMed: 10415601]

(17). Parks CG; de Souza Espindola Santos A; Barbhaiya M; Costenbader KH Understanding the role of environmental factors in the development of systemic lupus erythematosus. Best Pract Res. Clin Rheumatol 2017, 31, 306–320. [PubMed: 29224673]

(18). Sarzi-Puttini P; Atzeni F; Iaccarino L; Doria A Environment and systemic lupus erythematosus: An overview. Autoimmunity 2005, 38, 465–472. [PubMed: 16373251]

(19). Tofighi T; Morand EF; Touma Z Systemic lupus erythematosus outcome measures for systemic lupus erythematosus clinical trials. Rheum Dis Clin North Am. 2021, 47, 415–426. [PubMed: 34215371]

(20). He Y; Sawalha AH Drug-induced lupus erythematosus: An update on drugs and mechanisms. Curr. Opin Rheumatol 2018, 30, 490–497. [PubMed: 29870500]

(21). Bendiksen S; Van Ghelue M; Rekvig OP; Gutteberg T; Haga HJ; Moens U A longitudinal study of human cytomegalovirus serology and viruria fails to detect active viral infection in 20 systemic lupus erythematosus patients. Lupus 2000, 9, 120–126. [PubMed: 10787009]

(22). Roussou E; Iacovou C; Weerakoon A; Ahmed K Stress as a trigger of disease flares in sle. Rheumatology International 2013, 33, 1367–1370. [PubMed: 22193224]

(23). Morand EF Systemic lupus erythematosus: Stress and the onset of sle. Nat. Rev. Rheumatol 2018, 14, 127–128. [PubMed: 29367692]

(24). Harley IT; Kaufman KM; Langefeld CD; Harley JB; Kelly JA Genetic susceptibility to sle: New insights from fine mapping and genome-wide association studies. Nat. Rev. Genet 2009, 10, 285–290. [PubMed: 19337289]

Author Manuscript Author Manuscript Author Manuscript Author Manuscript

(25). Morel L Genetics of sle: Evidence from mouse models. Nat. Rev. Rheumatol 2010, 6, 348–357. [PubMed: 20440287]

(26). Block SR; Winfield JB; Lockshin MD; D'Angelo WA; Christian CL Studies of twins with systemic lupus erythematosus. A review of the literature and presentation of 12 additional sets. Am. J. Med 1975, 59, 533–552. [PubMed: 1101680]

(27). Prieto-Echague V; Gucwa A; Craddock BP; Brown DA; Miller WT Cancer-associated mutations activate the nonreceptor tyrosine kinase ack1. J. Biol. Chem 2010, 285, 10605–10615. [PubMed: 20110370]

(28). Gajiwala KS; Maegley K; Ferre R; He YA; Yu X Ack1: Activation and regulation by allostery. PLoS One 2013, 8, No. e53994. [PubMed: 23342057]

(29). Modi V; Dunbrack RL Jr. A structurally-validated multiple sequence alignment of 497 human protein kinase domains. Sci. Rep 2019, 9, 19790. [PubMed: 31875044]

(30). Fox M; Crafter C; Owen D The non-receptor tyrosine kinase ack: Regulatory mechanisms, signalling pathways and opportunities for attacking cancer. Biochem. Soc. Trans 2019, 47, 1715–1731. [PubMed: 31845724]

(31). Kelley LC; Weed SA Cortactin is a substrate of activated cdc42-associated kinase 1 (ack1) during ligand-induced epidermal growth factor receptor downregulation. PLoS One 2012, 7, e44363. [PubMed: 22952966]

(32). Mahajan K; Coppola D; Challa S; Fang B; Chen YA; Zhu W; Lopez AS; Koomen J; Engelman RW; Rivera C; Muraoka-Cook RS; Cheng JQ; Schonbrunn E; Sebti SM; Earp HS; Mahajan NP Ack1 mediated akt/pkb tyrosine 176 phosphorylation regulates its activation. PLoS One 2010, 5, e9646. [PubMed: 20333297]

(33). Mahajan K; Lawrence HR; Lawrence NJ; Mahajan NP Ack1 tyrosine kinase interacts with histone demethylase kdm3a to regulate the mammary tumor oncogene hoxa1. J. Biol. Chem 2014, 289, 28179–28191. [PubMed: 25148682]

(34). Mahendrarajah N; Borisova ME; Reichardt S; Godmann M; Sellmer A; Mahboobi S; Haitel A; Schmid K; Kenner L; Heinzel T; Beli P; Kramer OH Hsp90 is necessary for the ack1-dependent phosphorylation of stat1 and stat3. Cell Signal 2017, 39, 9–17. [PubMed: 28739485]

(35). Qiu H; Miller WT Role of the brk sh3 domain in substrate recognition. Oncogene 2004, 23, 2216–2223. [PubMed: 14676834]

(36). Qiu H; Miller WT Regulation of the nonreceptor tyrosine kinase brk by autophosphorylation and by autoinhibition. J. Biol. Chem 2002, 277, 34634–34641. [PubMed: 12121988]

(37). Born M; Quintanilla-Fend L; Braselmann H; Reich U; Richter M; Hutzler P; Aubele M Simultaneous over-expression of the her2/neu and ptk6 tyrosine kinases in archival invasive ductal breast carcinomas. J. Pathol 2005, 205, 592–596. [PubMed: 15685689]

(38). Ang HL; Yuan Y; Lai X; Tan TZ; Wang L; Huang BB; Pandey V; Huang RY; Lobie PE; Goh BC; Sethi G; Yap CT; Chan CW; Lee SC; Kumar AP Putting the brk on breast cancer: From molecular target to therapeutics. Theranostics 2021, 11 , 1115–1128. [PubMed: 33391524]

(39). Kasprzycka M; Majewski M; Wang ZJ; Ptasznik A; Wysocka M; Zhang Q; Marzec M; Gimotty P; Crompton MR; Wasik MA Expression and oncogenic role of brk (ptk6/sik) protein tyrosine kinase in lymphocytes. Am. J. Pathol 2006, 168, 1631–1641. [PubMed: 16651629]

(40). Liu C; Pan Z; Chen Q; Chen Z; Liu W; Wu L; Jiang M; Lin W; Zhang Y; Lin W; Zhou R; Zhao L Pharmacological targeting ptk6 inhibits the jak2/stat3 sustained stemness and reverses chemoresistance of colorectal cancer. J. Exp Clin Cancer Res 2021, 40, 297. [PubMed: 34551797]

(41). Jiao X; Kopecky DJ; Liu J; Liu J; Jaen JC; Cardozo MG; Sharma R; Walker N; Wesche H; Li S; Farrelly E; Xiao SH; Wang Z; Kayser F Synthesis and optimization of substituted furo[2,3-d]-pyrimidin-4-amines and 7h-pyrrolo[2,3-d]pyrimidin-4-amines as ack1 inhibitors. Bioorg. Med. Chem. Lett 2012, 22, 6212–6217. [PubMed: 22929232]

(42). Qiu L; Levine K; Gajiwala KS; Cronin CN; Nagata A; Johnson E; Kraus M; Tatlock J; Kania R; Foley T; Sun S Small molecule inhibitors reveal ptk6 kinase is not an oncogenic driver in breast cancers. PLoS One 2018, 13, e0198374. [PubMed: 29879184]

Author Manuscript Author Manuscript Author Manuscript Author Manuscript

(43). Liu Y; Shah K; Yang F; Witucki L; Shokat K A molecular gate which controls unnatural atp analogue recognition by the tyrosine kinase v-src. Bioorg. Med. Chem 1998, 6, 1219–1226. [PubMed: 9784863]

(44). Madhusudan; Akamine P; Xuong N-H; Taylor SS Crystal structure of a transition state mimic of the catalytic subunit of camp-dependent protein kinase. Nature structural biology 2002, 9, 273–277. [PubMed: 11896404]

(45). Yokoyama N; Miller WT Biochemical properties of the cdc42-associated tyrosine kinase ack1. Substrate specificity, authphosphorylation, and interaction with hck. J. Biol. Chem 2003, 278, 47713–47723. [PubMed: 14506255]

(46). Yokoyama N; Miller WT Purification and enzyme activity of ack1. Methods Enzymol 2006, 406, 250–260. [PubMed: 16472662]

(47). Kabsch W Integration, scaling, space-group assignment and post-refinement. Acta Crystallogr. D Biol. Crystallogr 2010, 66, 133–144. [PubMed: 20124693]

(48). Karplus PA; Diederichs K Linking crystallographic model and data quality. Science 2012, 336, 1030–1033. [PubMed: 22628654]

(49). Schwarzenbach D; Flack HD On the definition and practical use of crystal-based azimuthal angles. J. Appl. Crystallogr 1989, 22, 601–605.

(50). Diederichs K; Karplus PA Improved r-factors for diffraction data analysis in macromolecular crystallography. Nat. Struct. Biol 1997, 4, 269–275. [PubMed: 9095194]

(51). French S; Wilson K On the treatment of negative intensity observations. Acta Crystallogr., Sect. A 1978, 34, 517–525.

(52). Diederichs K; McSweeney S; Ravelli RB Zero-dose extrapolation as part of macromolecular synchrotron data reduction. Acta Crystallogr. D Biol. Crystallogr 2003, 59, 903–909. [PubMed: 12777808]

(53). Cowtan K 'Dm': An automated procedure for phase improvement by density modification. Joint CCP4 and ESF-EACBM Newsletter on Prorein Crystallogr 1994, 31, 34–38.

(54). Rossmann MG; Arnold E (2006) International Tables for Crystallography, Vol. F, Springer Dordrecht.

(55). Kabsch W Automatic processing of rotation diffraction data from crystals of initially unknown symmetry and cell constants. J. Appl. Crystallogr 1993, 26, 795–800.

(56). McCoy AJ; Grosse-Kunstleve RW; Adams PD; Winn MD; Storoni LC; Read RJ Phaser crystallographic software. J. Appl. Crystallogr 2007, 40, 658–674. [PubMed: 19461840]

(57). Emsley P; Cowtan K Coot: Model-building tools for molecular graphics. Acta Crystallogr. D Biol. Crystallogr 2004, 60, 2126–2132. [PubMed: 15572765]

(58). Liebschner D; Afonine PV; Baker ML; Bunkoczi G; Chen VB; Croll TI; Hintze B; Hung LW; Jain S; McCoy AJ; Moriarty NW; Oeffner RD; Poon BK; Prisant MG; Read RJ; Richardson JS; Richardson DC; Sammito MD; Sobolev OV; Stockwell DH; Terwilliger TC; Urzhumtsev AG; Videau LL; Williams CJ; Adams PD Macromolecular structure determination using x-rays, neutrons and electrons: Recent developments in phenix. Acta Crystallogr. D Struct Biol 2019, 75, 861–877. [PubMed: 31588918]

(59). Chen JE; Huang CC; Ferrin TE Rrdistmaps: A ucsf chimera tool for viewing and comparing protein distance maps. Bioinformatics 2015, 31, 1484–1486. [PubMed: 25540183]

(60). Waterhouse AM; Procter JB; Martin DM; Clamp M; Barton GJ Jalview version 2–a multiple sequence alignment editor and analysis workbench. Bioinformatics 2009, 25, 1189–1191. [PubMed: 19151095]

(61). Rodrigues CH; Pires DE; Ascher DB Dynamut: Predicting the impact of mutations on protein conformation, flexibility and stability. Nucleic Acids Res. 2018, 46, W350–W355. [PubMed: 29718330]

(62). Ng PC; Henikoff S Predicting deleterious amino acid substitutions. Genome Res. 2001, 11, 863–874. [PubMed: 11337480]

(63). Guerois R; Nielsen JE; Serrano L Predicting changes in the stability of proteins and protein complexes: A study of more than 1000 mutations. J. Mol. Biol 2002, 320, 369–387. [PubMed: 12079393]

Author Manuscript Author Manuscript Author Manuscript Author Manuscript

(64). Fariselli P; Martelli PL; Savojardo C; Casadio R Inps: Predicting the impact of non-synonymous variations on protein stability from sequence. Bioinformatics 2015, 31, 2816–2821. [PubMed: 25957347]

(65). Li G; Panday SK; Alexov E Saafec-seq: A sequence-based method for predicting the effect of single point mutations on protein thermodynamic stability. Int. J. Mol. Sci 2021, 22, 606. [PubMed: 33435356]

(66). Getov I; Petukh M; Alexov E Saafec: Predicting the effect of single point mutations on protein folding free energy using a knowledge-modified mm/pbsa approach. International journal of molecular sciences 2016, 17, 512. [PubMed: 27070572]

(67). Dehouck Y; Kwasigroch JM; Gilis D; Rooman M Popmusic 2.1: A web server for the estimation of protein stability changes upon mutation and sequence optimality. BMC Bioinformatics 2011, 12, 151. [PubMed: 21569468]

(68). Prieto-Echague V; Gucwa A; Brown DA; Miller WT Regulation of ack1 localization and activity by the amino-terminal sam domain. BMC Biochem 2010, 11, 42. [PubMed: 20979614]

(69). Casnellie JE Assay of protein kinases using peptides with basic residues for phosphocellulose binding. Methods Enzymol 1991, 200, 115–120. [PubMed: 1956315]

(70). Yue P; Li Z; Moult J Loss of protein structure stability as a major causative factor in monogenic disease. J. Mol. Biol 2005, 353, 459–473. [PubMed: 16169011]

(71). Taylor SS; Shaw AS; Kannan N; Kornev AP Integration of signaling in the kinome: Architecture and regulation of the alphac helix. Biochim. Biophys. Acta 2015, 1854, 1567–1574. [PubMed: 25891902]

(72). Hu J; Ahuja LG; Meharena HS; Kannan N; Kornev AP; Taylor SS; Shaw AS Kinase regulation by hydrophobic spine assembly in cancer. Mol. Cell. Biol 2015, 35, 264–276. [PubMed: 25348715]

(73). Kim J; Ahuja LG; Chao FA; Xia Y; McClendon CL; Kornev AP; Taylor SS; Veglia G A dynamic hydrophobic core orchestrates allostery in protein kinases. Sci. Adv 2017, 3, e1600663. [PubMed: 28435869]

(74). Cao H; Wang J; He L; Qi Y; Zhang JZ Deepddg: Predicting the stability change of protein point mutations using neural networks. J. Chem. Inf Model 2019, 59, 1508–1514. [PubMed: 30759982]

(75). Khan S; Vihinen M Performance of protein stability predictors. Human Mutation 2010, 31, 675–684. [PubMed: 20232415]

(76). Stefl S; Nishi H; Petukh M; Panchenko AR; Alexov E Molecular mechanisms of disease-causing missense mutations. J. Mol. Biol 2013, 425, 3919–3936. [PubMed: 23871686]

(77). Liu J; McCleland M; Stawiski EW; Gnad F; Mayba O; Haverty PM; Durinck S; Chen YJ; Klijn C; Jhunjhunwala S; Lawrence M; Liu H; Wan Y; Chopra V; Yaylaoglu MB; Yuan W; Ha C; Gilbert HN; Reeder J; Pau G; Stinson J; Stern HM; Manning G; Wu TD; Neve RM; de Sauvage FJ; Modrusan Z; Seshagiri S; Firestein R; Zhang Z Integrated exome and transcriptome sequencing reveals zak isoform usage in gastric cancer. Nat. Commun 2014, 5, 3830. [PubMed: 24807215]

(78). Soverini S; De Benedittis C; Machova Polakova K; Brouckova A; Horner D; Iacono M; Castagnetti F; Gugliotta G; Palandri F; Papayannidis C; Iacobucci I; Venturi C; Bochicchio MT; Klamova H; Cattina F; Russo D; Bresciani P; Binotto G; Giannini B; Kohlmann A; Haferlach T; Roller A; Rosti G; Cavo M; Baccarani M; Martinelli G Unraveling the complexity of tyrosine kinase inhibitor-resistant populations by ultradeep sequencing of the bcr-abl kinase domain. Blood 2013, 122, 1634–1648. [PubMed: 23794064]

(79). Chen X; Stewart E; Shelat AA; Qu C; Bahrami A; Hatley M; Wu G; Bradley C; McEvoy J; Pappo A; Spunt S; Valentine MB; Valentine V; Krafcik F; Lang WH; Wierdl M; Tsurkan L; Tolleman V; Federico SM; Morton C; Lu C; Ding L; Easton J; Rusch M; Nagahawatte P; Wang J; Parker M; Wei L; Hedlund E; Finkelstein D; Edmonson M; Shurtleff S; Boggs K; Mulder H; Yergeau D; Skapek S; Hawkins DS; Ramirez N; Potter PM; Sandoval JA; Davidoff AM; Mardis ER; Wilson RK; Zhang J; Downing JR; Dyer MA St. Jude Children's Research Hospital-Washington University Pediatric Cancer Genome, P. Targeting oxidative stress in embryonal rhabdomyosarcoma. Cancer Cell 2013, 24, 710–724. [PubMed: 24332040]

Author Manuscript Author Manuscript Author Manuscript Author Manuscript

(80). Keller J; Shroyer KR; Batajoo SK; Zhao HL; Dong LM; Hayman MJ; Chan EL Combination of phosphorylated and truncated egfr correlates with higher tumor and nodal stage in head and neck cancer. Cancer Invest 2010, 28, 1054–1062. [PubMed: 20873989]

(81). Shah SP; Roth A; Goya R; Oloumi A; Ha G; Zhao Y; Turashvili G; Ding J; Tse K; Haffari G; Bashashati A; Prentice LM; Khattra J; Burleigh A; Yap D; Bernard V; McPherson A; Shumansky K; Crisan A; Giuliany R; Heravi-Moussavi A; Rosner J; Lai D; Birol I; Varhol R; Tam A; Dhalla N; Zeng T; Ma K; Chan SK; Griffith M; Moradian A; Cheng SW; Morin GB; Watson P; Gelmon K; Chia S; Chin SF; Curtis C; Rueda OM; Pharoah PD; Damaraju S; Mackey J; Hoon K; Harkins T; Tadigotla V; Sigaroudinia M; Gascard P; Tlsty T; Costello JF; Meyer IM; Eaves CJ; Wasserman WW; Jones S; Huntsman D; Hirst M; Caldas C; Marra MA; Aparicio S The clonal and mutational evolution spectrum of primary triple-negative breast cancers. Nature 2012, 486, 395–399. [PubMed: 22495314]

(82). Gingras MC; Covington KR; Chang DK; Donehower LA; Gill AJ; Ittmann MM; Creighton CJ; Johns AL; Shinbrot D; Dewal N; Fisher WE; Australian Pancreatic Cancer Genome, I.; Pilarsky C; Grutzmann R; Overman MJ; Jamieson NB; Van Buren G 2nd; Drummond J; Walker K; Hampton OA; Xi L; Muzny DM; Doddapaneni H; Lee SL; Bellair M; Hu J; Han Y; Dinh HH; Dahdouli M; Samra JS; Bailey P; Waddell N; Pearson JV; Harliwong I; Wang H; Aust D; Oien KA; Hruban RH; Hodges SE; McElhany A; Saengboonmee C; Duthie FR; Grimmond SM; Biankin AV; Wheeler DA; Gibbs RA (2016) Ampullary cancers harbor elf3 tumor suppressor gene mutations and exhibit frequent wnt dysregulation. Cell Rep 14, 907–919. [PubMed: 26804919]

(83). Crompton BD; Stewart C; Taylor-Weiner A; Alexe G; Kurek KC; Calicchio ML; Kiezun A; Carter SL; Shukla SA; Mehta SS; Thorner AR; de Torres C; Lavarino C; Sunol M; McKenna A; Sivachenko A; Cibulskis K; Lawrence MS; Stojanov P; Rosenberg M; Ambrogio L; Auclair D; Seepo S; Blumenstiel B; DeFelice M; Imaz-Rosshandler I; Schwarz-Cruz y Celis A; Rivera MN; Rodriguez-Galindo C; Fleming MD; Golub TR; Getz G; Mora J; Stegmaier K The genomic landscape of pediatric ewing sarcoma. Cancer Discov 2014, 4, 1326–1341. [PubMed: 25186949]

(84). Azam M; Latek RR; Daley GQ Mechanisms of autoinhibition and sti-571/imatinib resistance revealed by mutagenesis of bcr-abl. Cell 2003, 112, 831–843. [PubMed: 12654249]

(85). Azam M; Raz T; Nardi V; Opitz SL; Daley GQ A screen to identify drug resistant variants to target-directed anti-cancer agents. Biol. Proced Online 2003, 5, 204–210. [PubMed: 14615817]

(86). Scarlett CJ; Salisbury EL; Biankin AV; Kench J Precursor lesions in pancreatic cancer: Morphological and molecular pathology. Pathology 2011, 43, 183–200. [PubMed: 21436628]

(87). Pinter F; Papay J; Almasi A; Sapi Z; Szabo E; Kanya M; Tamasi A; Jori B; Varkondi E; Moldvay J; Szondy K; Keri G; Dominici M; Conte P; Eckhardt S; Kopper L; Schwab R; Petak H Epidermal growth factor receptor (egfr) high gene copy number and activating mutations in lung adenocarcinomas are not consistently accompanied by positivity for egfr protein by standard immunohistochemistry. Journal of molecular diagnostics: JMD 2008, 10, 160–168. [PubMed: 18258923]

(88). Yi S; Zhuang Y; Zhou J; Ma H; Huang J; Wang L; Zhu W; Kang S; Guo L; Guo F A comparison of epidermal growth factor receptor mutation testing methods in different tissue types in non-small cell lung cancer. Int. J. Mol. Med 2014, 34, 464–474. [PubMed: 24891042]

(89). Sawada G; Niida A; Uchi R; Hirata H; Shimamura T; Suzuki Y; Shiraishi Y; Chiba K; Imoto S; Takahashi Y; Iwaya T; Sudo T; Hayashi T; Takai H; Kawasaki Y; Matsukawa T; Eguchi H; Sugimachi K; Tanaka F; Suzuki H; Yamamoto K; Ishii H; Shimizu M; Yamazaki H; Yamazaki M; Tachimori Y; Kajiyama Y; Natsugoe S; Fujita H; Mafune K; Tanaka Y; Kelsell DP; Scott CA; Tsuji S; Yachida S; Shibata T; Sugano S; Doki Y; Akiyama T; Aburatani H; Ogawa S; Miyano S; Mori M; Mimori K Genomic landscape of esophageal squamous cell carcinoma in a japanese population. Gastroenterology 2016, 150, 1171–1182. [PubMed: 26873401]

(90). Liu Y; Wu BQ; Zhong HH; Hui P; Fang WG Screening for egfr and kras mutations in non-small cell lung carcinomas using DNA extraction by hydrothermal pressure coupled with pcr-based direct sequencing. Int. J. Clin Exp Pathol 2013, 6, 1880–1889. [PubMed: 24040454]

(91). Zehir A; Benayed R; Shah RH; Syed A; Middha S; Kim HR; Srinivasan P; Gao J; Chakravarty D; Devlin SM; Hellmann MD; Barron DA; Schram AM; Hameed M; Dogan S; Ross DS; Hechtman JF; DeLair DF; Yao J; Mandelker DL; Cheng DT; Chandramohan R; Mohanty AS; Ptashkin

Author Manuscript Author Manuscript Author Manuscript Author Manuscript

RN; Jayakumaran G; Prasad M; Syed MH; Rema AB; Liu ZY; Nafa K; Borsu L; Sadowska J; Casanova J; Bacares R; Kiecka IH; Razumova A; Son JB; Stewart L; Baldi T; Mullaney KA; Al-Ahmadie H; Vakiani E; Abeshouse AA; Penson AV; Jonsson P; Camacho N; Chang MT; Won HH; Gross BE; Kundra R; Heins ZJ; Chen HW; Phillips S; Zhang H; Wang J; Ochoa A; Wills J; Eubank M; Thomas SB; Gardos SM; Reales DN; Galle J; Durany R; Cambria R; Abida W; Cercek A; Feldman DR; Gounder MM; Hakimi AA; Harding JJ; Iyer G; Janjigian YY; Jordan EJ; Kelly CM; Lowery MA; Morris LGT; Omuro AM; Raj N; Razavi P; Shoushtari AN; Shukla N; Soumerai TE; Varghese AM; Yaeger R; Coleman J; Bochner B; Riely GJ; Saltz LB; Scher HI; Sabbatini PJ; Robson ME; Klimstra DS; Taylor BS; Baselga J; Schultz N; Hyman DM; Arcila ME; Solit DB; Ladanyi M; Berger MF Mutational landscape of metastatic cancer revealed from prospective clinical sequencing of 10,000 patients. Nat. Med 2017, 23, 703–713. [PubMed: 28481359]

(92). Li AR; Chitale D; Riely GJ; Pao W; Miller VA; Zakowski MF; Rusch V; Kris MG; Ladanyi M Egfr mutations in lung adenocarcinomas: Clinical testing experience and relationship to egfr gene copy number and immunohistochemical expression. J. Mol. Diagn 2008, 10, 242–248. [PubMed: 18403609]

(93). The Cancer Genome Atlas Network. Comprehensive molecular portraits of human breast tumours. Nature 2012, 490, 61–70. [PubMed: 23000897]

(94). The Cancer Genome Atlas Network. Comprehensive molecular characterization of human colon and rectal cancer. Nature 2012, 487, 330–337. [PubMed: 22810696]

(95). Giannakis M; Mu XJ; Shukla SA; Qian ZR; Cohen O; Nishihara R; Bahl S; Cao Y; Amin-Mansour A; Yamauchi M; Sukawa Y; Stewart C; Rosenberg M; Mima K; Inamura K; Nosho K; Nowak JA; Lawrence MS; Giovannucci EL; Chan AT; Ng K; Meyerhardt JA; Van Allen EM; Getz G; Gabriel SB; Lander ES; Wu CJ; Fuchs CS; Ogino S; Garraway LA Genomic correlates of immune-cell infiltrates in colorectal carcinoma. Cell Rep 2016, 15, 857–865. [PubMed: 27149842]

(96). Seshagiri S; Stawiski EW; Durinck S; Modrusan Z; Storm BE; Conboy CB; Chaudhuri S; Guan Y; Janakiraman V; Jaiswal BS; Guillory J; Ha C; Dijkgraaf GJ; Stinson J; Gnad F; Huntley MA; Degenhardt JD; Haverty PM; Bourgon R; Wang W; Koeppen H; Gentleman R; Starr TK; Zhang Z; Largaespada DA; Wu TD; de Sauvage FJ Recurrent r-spondin fusions in colon cancer. Nature 2012, 488, 660–664. [PubMed: 22895193]

(97). Huang SF; Liu HP; Li LH; Ku YC; Fu YN; Tsai HY; Chen YT; Lin YF; Chang WC; Kuo HP; Wu YC; Chen YR; Tsai SF High frequency of epidermal growth factor receptor mutations with complex patterns in non-small cell lung cancers related to gefitinib responsiveness in taiwan. Clin. Cancer Res 2004, 10, 8195–8203. [PubMed: 15623594]

(98). Yamamoto G; Kikuchi M; Kobayashi S; Arai Y; Fujiyoshi K; Wakatsuki T; Kakuta M; Yamane Y; Iijima Y; Mizutani H; Nakajima Y; Sudo J; Kinoshita H; Kurimoto F; Akiyama H; Uramoto H; Sakai H; Akagi Y; Akagi K Routine genetic testing of lung cancer specimens derived from surgery, bronchoscopy and fluid aspiration by next generation sequencing. Int. J. Oncol 2017, 50, 1579–1589. [PubMed: 28350094]

(99). Jing L; Zhang X; Liu D; Yang Y; Xiong H; Dong G Ack1 contributes to the pathogenesis of inflammation and autoimmunity by promoting the activation of tlr signaling pathways. Front Immunol 2022, 13, 864995. [PubMed: 35669783]

(100). Ji Z; Njauw CN; Guhan S; Kumar R; Reddy B; Rajadurai A; Flaherty K; Tsao H Loss of ack1 upregulates egfr and mediates resistance to braf inhibition. J. Invest Dermatol 2021, 141, 1317–1324. [PubMed: 33159968]

Author Manuscript Author Manuscript Author Manuscript Author Manuscript

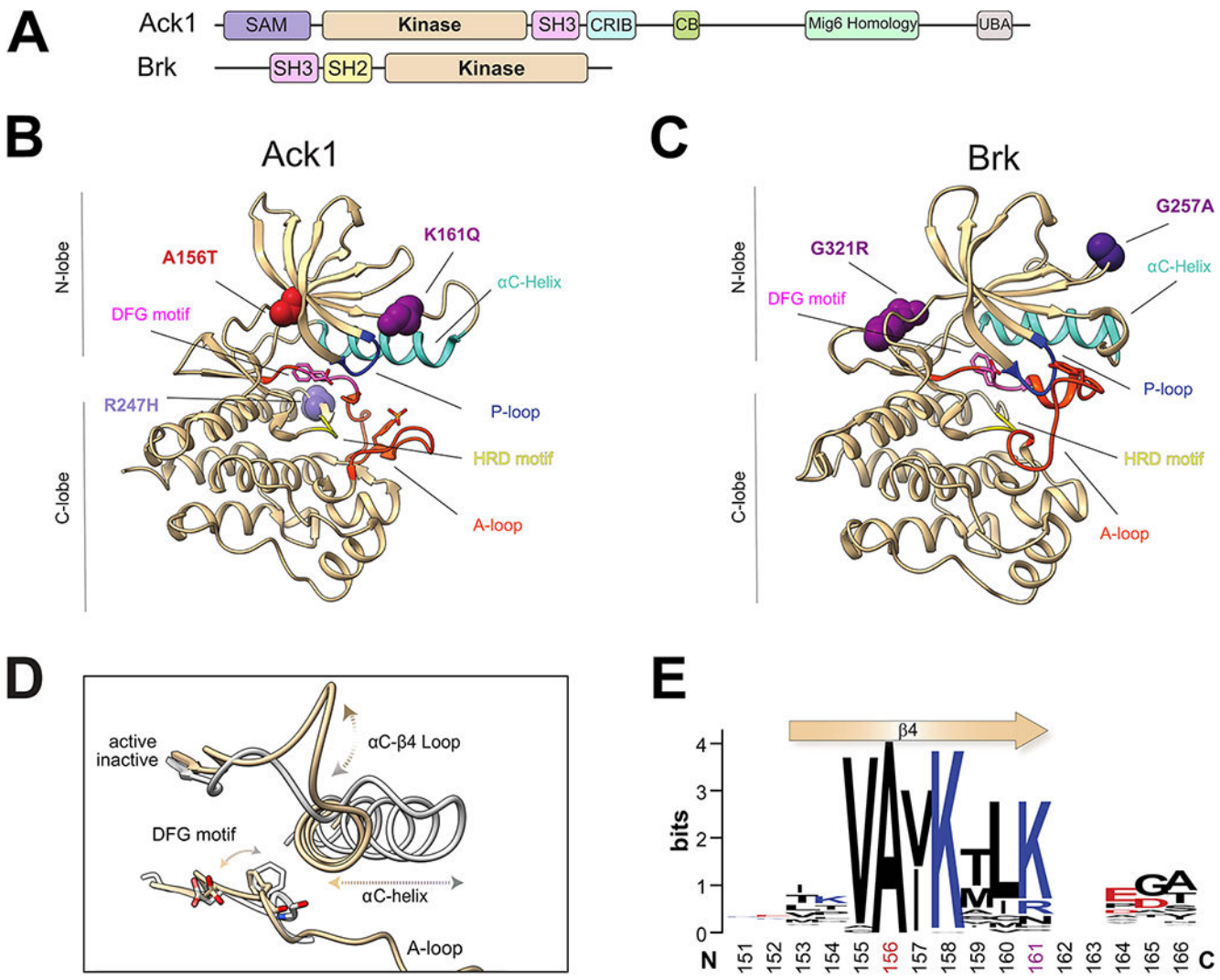

Figure 1.

Overview of SLE-associated mutations on crystal structures. (A) Domain organization of Ack1 (top) and Brk (bottom). SAM, sterile alpha motif; CRIB, Cdc42, and Rac1 binding; CB, clathrin-binding; UBA, ubiquitin-associated domain. Ribbon diagrams of (B) the active wild-type Ack1 KD (PDB: 4EWH, beige) and (C) Brk KD (PDB: 6CZ3, beige) structures depicting the position of the mutations relative to the common structural elements shared within the NRTKs: A-loop, activation loop (orange); P-loop, phosphate-binding loop (navy); DFG motif, Asp-Phe-Gly motif that coordinates magnesium binding (pink); and HRD motif, His-Arg-Asp catalytic triad (yellow). The activation loop autophosphorylation sites (Y284 for Ack1; Y342 for Brk) and the DFG motif are shown as sticks. Mutations are color-coded as follows: Ack1 A156T (dark red), K161Q (purple), R247H (dark blue); Brk G321R (purple), and G257A (dark blue). (D) The structural differences between active and inactive Ack1 KD conformations near the C helix. The C helix of the active structure (from panel B) is shown in beige, while that of the inactive structure (PDB: 4HZR) is shown in gray. (E) Sequence logo for the region encompassing A156 and K161 of Ack1 and its

Author Manuscript Author Manuscript Author Manuscript Author Manuscript

conservation among nonreceptor tyrosine kinases, generated using Modi and Dunbrack's[29] multiple sequence alignment as input. The residues are numbered according to their position in Ack1.

Author Manuscript Author Manuscript Author Manuscript Author Manuscript

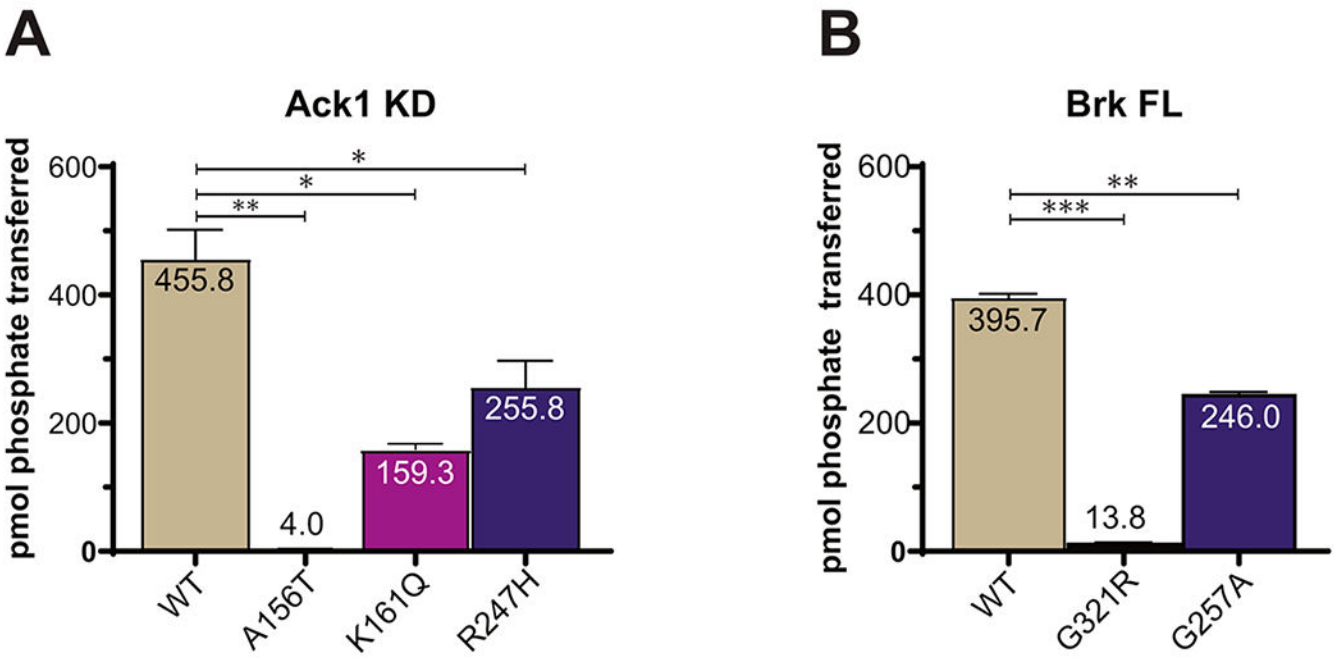

Figure 2.

Activities of SLE-associated Ack1 and Brk mutants. Catalytic activity of the isolated (A) Ack1 kinase domain and (B) full-length Brk proteins harboring the SLE-associated mutations (color-coded according to Figure 1) was measured using the phosphocellulose paper binding assay[69] and a peptide substrate. The WASP peptide[46] was used as a substrate for Ack1 KD, while the Src peptide[36] was used in reactions with full-length Brk.

Author Manuscript Author Manuscript Author Manuscript Author Manuscript

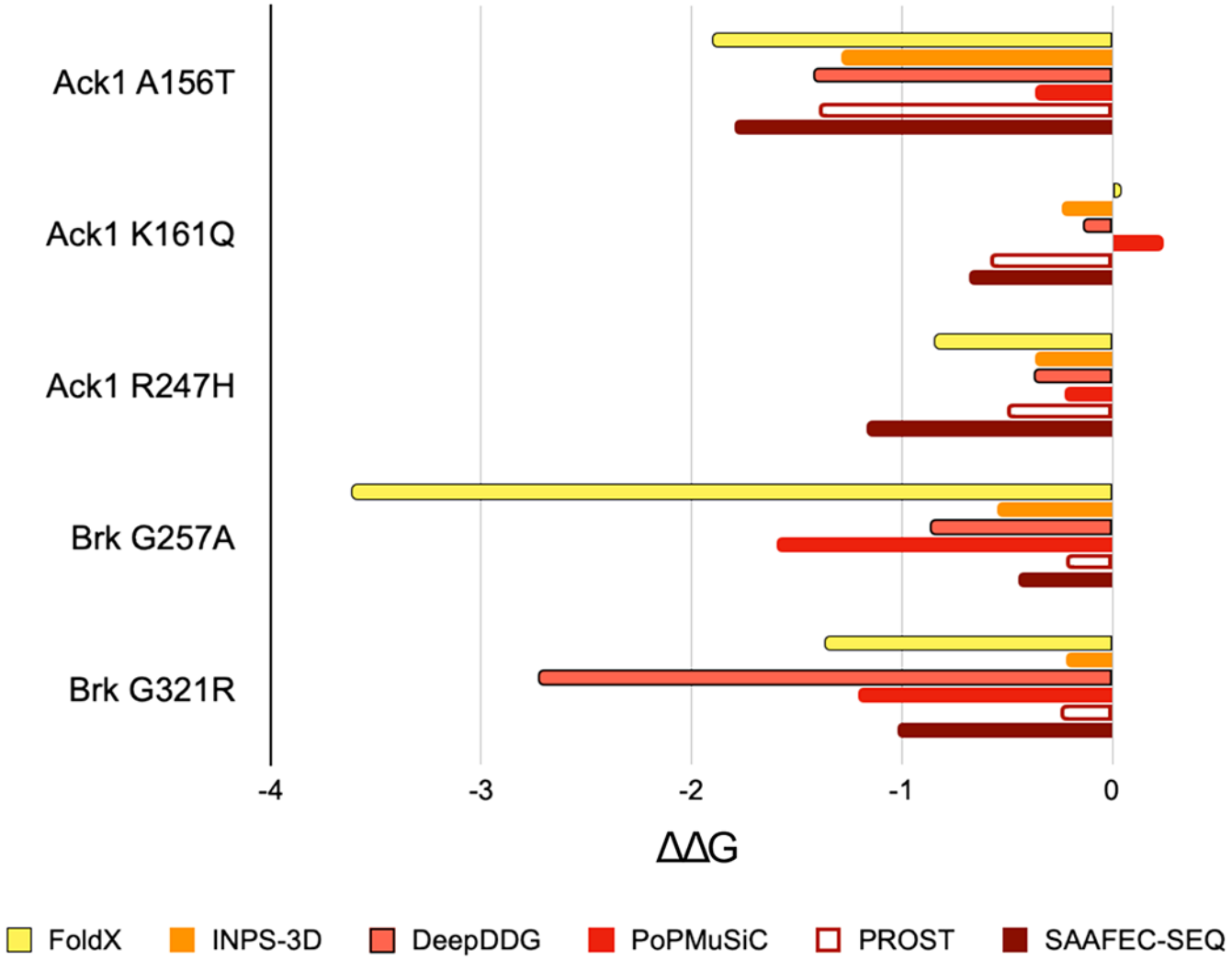

Figure 3.

In silico prediction of the effects of the mutations. Folding free energy change ($\Delta\Delta G$) between wild-type and mutant proteins calculated by FoldX (yellow bars), INPS-3D (orange bars), DeepDDG (orange bars with black outlines), PoPMuSiC (red), PROST (white bars with dark red outlines), and SAAFEC-SEQ (dark red bars) servers using various algorithms. The output of these tools is reported in kcal/mol. A $\Delta\Delta G$ value < 0 indicates a destabilizing mutation.

Author Manuscript Author Manuscript Author Manuscript Author Manuscript

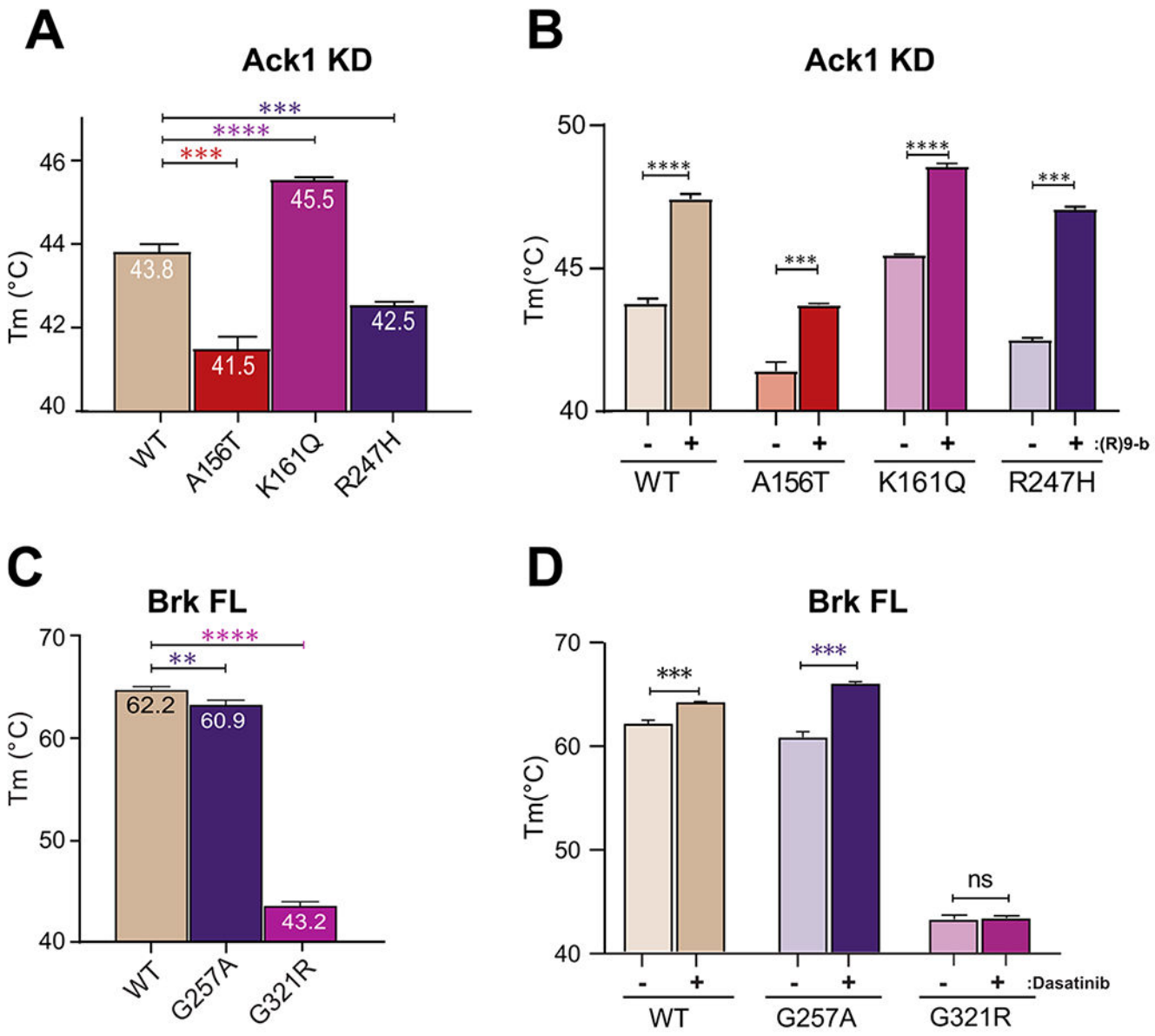

Figure 4.

Determination of the melting temperatures of Ack1 KD or Brk FL proteins that carry SLE-associated mutants. (A) Comparison of the melting temperatures of WT Ack1 (beige) and the SLE-associated mutants A156T (dark red), K161Q (purple), and R247H (dark blue). (B) Comparison of the melting temperatures of WT Ack1 (beige) and SLE-associated mutants with the addition of an ATP-competitive inhibitor (R)-9b. The increase in T_m with the addition of (R)-9b indicates the binding of the inhibitor to the mutants. (C) Comparison of the melting temperatures of WT Brk (beige) and the SLE-associated mutants G257A (dark blue) and G257A (purple). (D) Comparison of the melting temperatures of WT Brk (beige) and the SLE-associated mutants G257A (dark blue) and G321R (purple) with the addition of the ATP competitive inhibitor dasatinib. The increase in T_m with the addition of dasatinib indicates the binding of the inhibitor to the mutant. Melting temperatures were

Author Manuscript Author Manuscript Author Manuscript Author Manuscript

determined using the thermal shift assay. A two-tailed *t* test was used to determine whether the difference in temperature changes was statistically significant. A *p*-value < 0.05 was used as a criterion for statistical significance (**** $p < 0.0001$, *** $p < 0.001$, ** $p < 0.01$, * $p < 0.05$, ns: $p > 0.05$).

Author Manuscript Author Manuscript Author Manuscript Author Manuscript

A

Enzyme		k_{cat} (min^{-1})*	K_m (ATP, μM)*	k_{cat}/K_m (μM^{-1} min^{-1})*
Ack1 KD	WT	7.46 ± 0.58	196.5 ± 20.6	0.04 ± 0.01
	A156T	nd	nd	nd
	K161Q	2.98 ± 0.18	339.7 ± 42.6	0.01
	R247H	2.06 ± 0.16	131 ± 29	0.02
Brk FL	WT	14.5 ± 0.67	178.9 ± 20.5	0.08 ± 0.01
	G257A	13.5 ± 1.1	250.1 ± 65.1	0.06 ± 0.02
	G321R	nd	nd	nd

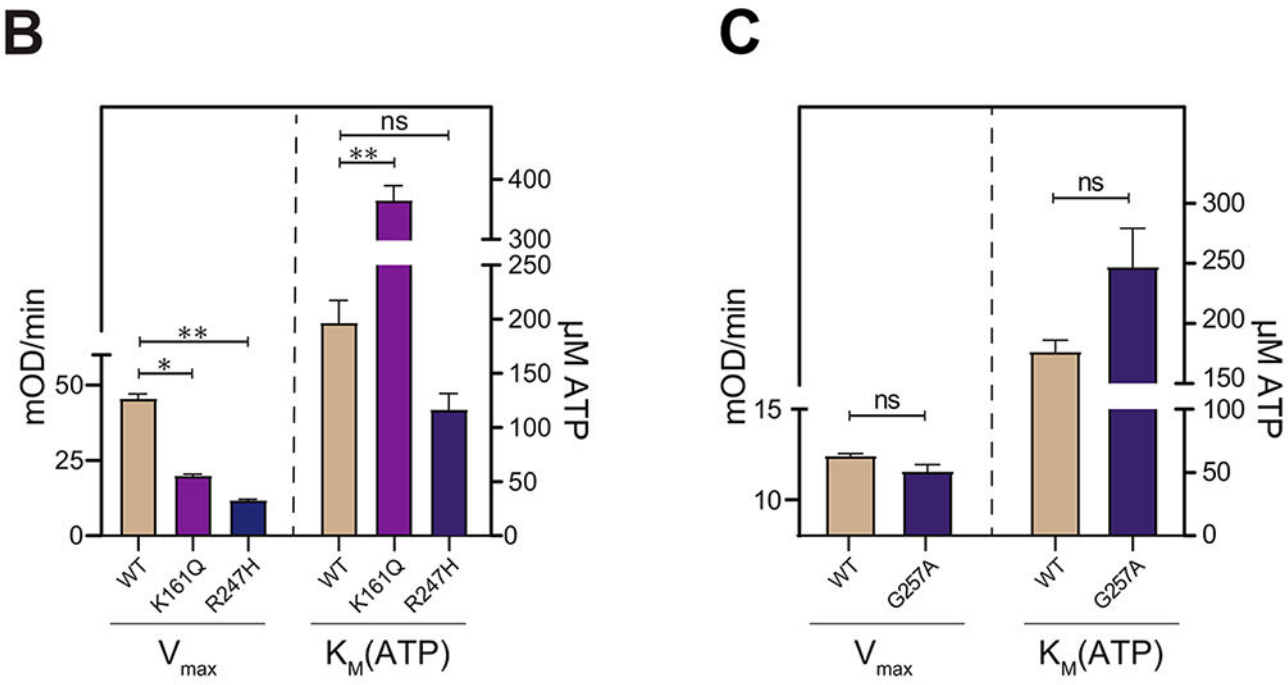

Figure 5.

Characterization and activity comparisons of wild type and mutant Ack1 and Brk proteins associated with SLE. (A) Kinetic parameters determined using the continuous spectrophotometric assay. nd, Not detectable. ATP concentrations ranged from 25 μM to 1.5 mM. The rates were replotted against ATP concentration and fitted to the Michaelis–Menten equation (Figure S3). Assays were carried out with 0.5 μM enzyme and 1 mM substrate. Absorbance data were recorded every 8 s. Values are ± SD. (B) Initial rates were measured

at various concentrations of WASP peptide using the continuous assay. (C) Initial rates were measured at various concentrations of Src peptide using the continuous assay.

Author Manuscript Author Manuscript Author Manuscript Author Manuscript

Author Manuscript Author Manuscript Author Manuscript Author Manuscript

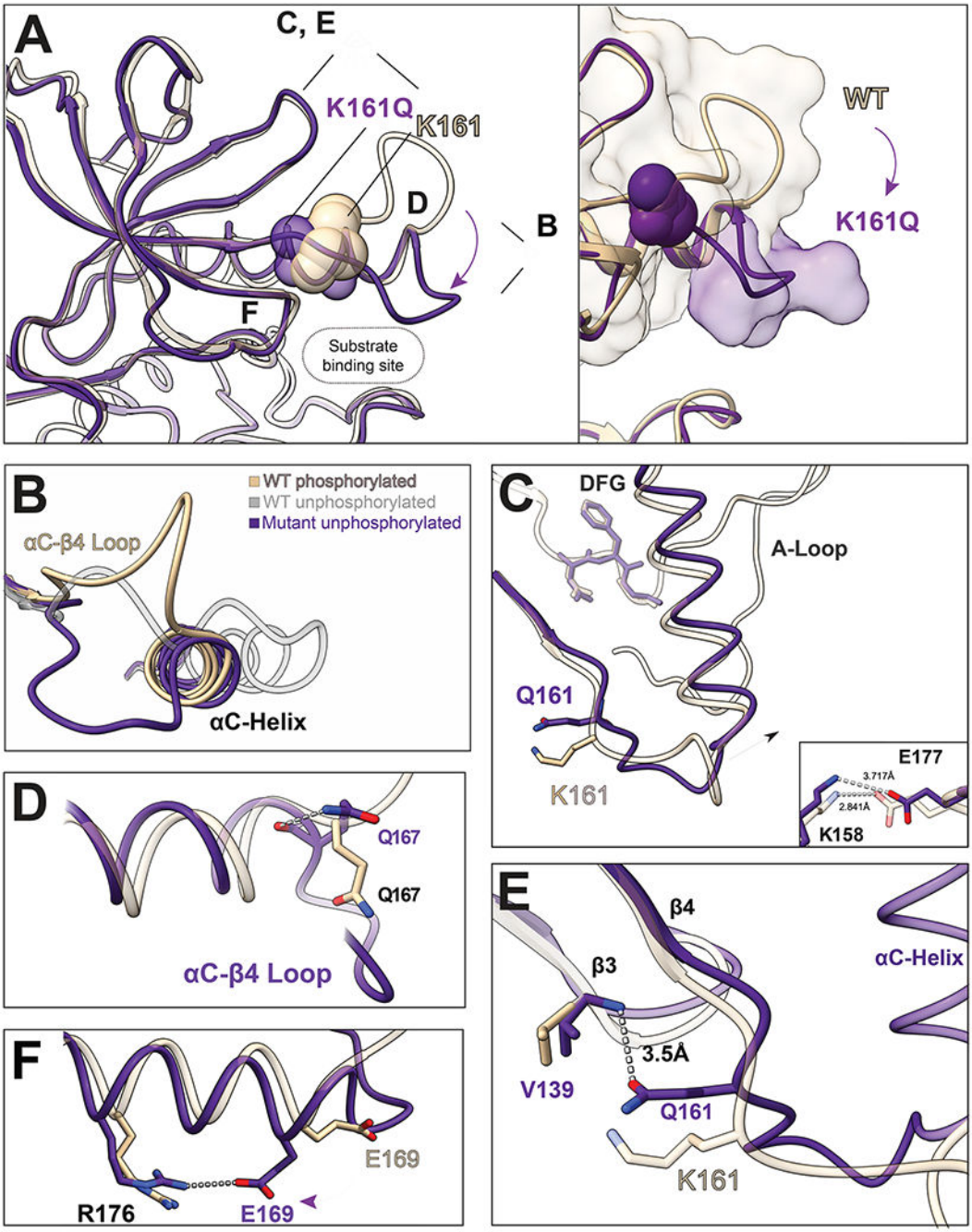

Figure 6.

Crystallographic studies of Ack1 KD K161Q. (A) Overview of the conformational changes introduced by the mutation. The crystal structure of Ack1 KD K161Q (purple) superimposed on the active autophosphorylated WT structure (PDB: 4EWH, beige) is depicted as a ribbon diagram. (A) Left: The location of panels B–F is mapped onto the ribbon diagram structure of K161Q. Right: The mutation causes the αC-β4 loop to flip, leading to a partial blockage of the substrate-binding site. (B) Comparison of the position of the αC helix in WT phosphorylated (beige) and unphosphorylated (gray) structures vs K161Q (purple). (C)

The shift in the αC helix introduces new H bonds between (D) the side chain nitrogen of Gln 167 and its backbone carbonyl oxygen, and (E) Val 139 and Gln 161. (F) The shift in the αC helix favors the Glu 169–Arg 176 salt bridge.

Author Manuscript Author Manuscript Author Manuscript Author Manuscript

Author Manuscript Author Manuscript Author Manuscript Author Manuscript

Table 1.

Data Collection and Refinement Statistics for Ack1 KD K161Q

Data collection	
wavelength (Å)	0.97933
Space Group	*I*422
a, b, c Cell Dimensions (Å)	91.69, 91.69, 190.07
Resolution (Å)	28.99–3.19 (3.28–3.19)[a]
R Merge	0.148 (1.088)[a]
$I/\Sigma i$	19.60 (2.40)[a]
Completeness (%)	99.1 (90.0)[a]
Multiplicity	25.1 (19.3)[a]
Number of Measured Reflections	176464
Number of Unique Reflections	7020
Refinement	
Method	molecular replacement
Resolution (Å)	28.99–3.2
Free *R* Test Set Size (#/%)	700/10
R_{work}/R_{free}	0.2005/0.2534
No. Atoms	
Protein	2205
Ligand	39
Average B-Factors	106.4
RMSD From Ideality	
Bonds (Å)	0.002
Angles (deg)	0.563
Ramachandran Statistics	
Favored (%)	96.34
Disallowed (%)	0
Molprobity	
Clash Score	3.60
Overall Score	1.40

[a]Numbers in parentheses refer to the highest-resolution shell.

Author Manuscript Author Manuscript Author Manuscript Author Manuscript

Table 2.

Analogous Disease-Associated Mutations within Other Tyrosine Kinases[a]

			Ack1 K161Q	
Abl	K274	E	Chronic myeloid leukemia (dasatinib-resistant)	78
Csk	K225	T	Rhabdomyosarcoma	79
EGFR	R748	I	Head and neck cancer	80
Frk	K265	R	Triple-negative breast cancer	81
ITK	R394	W	Ampullary cancer	82
			Ack1 R247H	
EGFR	R832	H	Ewing's sarcoma	83
			Ack1 A156T	
Abl	A269	T	Acute lymphoblastic leukemia (Ph+)	78
Abl	A269	V	Chronic lymphoblastic leukemia (Ph+)	84,85
Csk	A220	T	Pancreatic cancer	86
EGFR	A743	T	Nonsmall cell lung cancer (NSCLC) lung adenocarcinoma	87,88
EGFR	A743	V	NSCLC, esophageal squamous cell carcinoma	89–91
FGFR3	A508	T	Skin squamous cell carcinoma	92
FGFR3	A508	V	Skin squamous cell carcinoma	91
FGFR4	A484	T	Breast invasive carcinoma	93
Ret	A756	V	Colon cancer	94
Srms	A256	T	Colon cancer	95
Tec	A396	T	Colon cancer	96
			Brk G321R	
Abl (1a)	G372	R	Chronic myeloid leukemia (Ph+)	85
Abl (1b)	G391	R	Chronic myeloid leukemia (Ph+)	85
EGFR	K846	R	NSCLC	97

[a]All TKs possessing a residue homologous to the SLE-associated mutations (90 members) were searched in the COSMIC database. The first column indicates the name of the proteins followed by the corresponding residue. The third column shows the substitution mutation, with the disease the mutation was documented in the following column.

Ph+, Philadelphia chromosome-positive.